

# Adaptive cluster approximation for reduced density-matrix functional theory

Robert Schade<sup>1,\*</sup> and Peter E. Blöchl<sup>1,2</sup>

<sup>1</sup>*Institute for Theoretical Physics, Clausthal University of Technology,  
Leibnizstr. 10, 38678 Clausthal-Zellerfeld, Germany*

<sup>2</sup>*Institute for Materials Physics, Georg-August-Universität Göttingen,  
Friedrich-Hund-Platz 1, 37077 Göttingen, Germany*

(Dated: December 21, 2016)

The exact reduced density-matrix functional for interacting electrons can in principle be calculated from Levy's constrained search formalism. In order to make the problem tractable it is divided into impurity problems, where the impurity captures the interaction. A method, called the adaptive cluster approximation (ACA), is proposed to concentrate the effect of the bath to a small cluster around the impurity. A unitary transformation between the bath basis states is tailored to minimize the deviations introduced by truncating the set of bath states. The reduced density-matrix functional for the resulting cluster is evaluated using Levy's constrained search over an ensemble of fermionic many-particle wave functions. The method is evaluated for single-impurity Anderson models with finite baths and finite Hubbard rings. The method converges rapidly to the exact result with the size of the effective bath.

PACS numbers: 71.15.-m, 71.10.Fd, 71.27.+a

Keywords: reduced density-matrix functional theory, local approximation, Hubbard model, Anderson impurity model, Cluster methods, Variational approach

## I. INTRODUCTION

Reduced density-matrix functional theory<sup>1-3</sup> (rDMFT) emerged recently as viable option to describe materials with strong electronic correlations. It can be seen as a relative to density-functional theory<sup>4,5</sup> (DFT) that instead of the electron density treats the one-particle reduced density matrix as the basic quantity. In this sense rDMFT emphasizes orbital occupations that are more natural for the description of correlated materials.

Like the exchange-correlation functional of DFT the effort to evaluate the exact reduced density-matrix functional is expensive. Different strategies have been used to cope with this problem:

Analogous to DFT, the many-particle problem can be encoded in approximate, parameterized density-matrix functionals that can be evaluated with a small computational effort. Parametrized functionals have been applied to models<sup>6-17</sup> and real systems<sup>18-32</sup>.

Levy's constrained-search algorithm<sup>2,33</sup> describes a constrained optimization problem in the space of many-particle wave functions. This method inherits the difficulties of the many-particle problem. While numerically exact it is restricted to rather small system sizes in practice.

Functionals that involve the solution of an optimization problem like Levy's constrained-search algorithm suffer from a unfavorable scaling of the computational complexity with the total system size.

Cluster approximations are therefore vital to make the problem tractable. Impurity approximations limit the two-particle interaction to a small portion of the cluster. This portion of the cluster, i.e. one-particle basis states with a two-particle interaction, is called the impurity.

Basis states without a two-particle interaction are defined as the bath.

Even though the interaction is limited to a few one-particle basis states, the entire cluster is a many-particle quantum problem. Therefore methods that allow to minimize the cluster size are highly desirable.

An example for such an approach is the two-level approximation<sup>14,34</sup> by Töws et al. The main idea of the two-level-approximation is to introduce a unitary transformation of the bath states, such that only two of the transformed bath states have finite density-matrix elements with the impurity. All other basis states are neglected, which gives an effective system of four basis states, two impurity states and two basis states, for which the density-matrix functional is known. Consequently the two-level-approximation is limited to impurities with two spin-orbitals and an effective bath consisting of two spin-orbitals.

In this paper we introduce a method, named adaptive cluster approximation (ACA), that can handle impurity problems with an arbitrary number of effective bath states/levels, arbitrary impurity sizes and multi-band interactions. The method sets up a unitary transformation between the non-interacting basis states, that aims at minimizing the subsequent truncation error of bath states.

The paper is organized as follows. In section II, we first describe the local approximation as one method to divide an extended many-particle problem into local impurity problems. Then we present the theoretical foundation of the ACA. We describe relations to existing methods and present exact limits. In section III the numerical methodology is presented. In section IV we describe applications of the method. We first investigate a simple single-impurity Anderson model (SIAM) with a finite bath for which we can obtain the numerically exact ground state

from exact diagonalization. We explore the dependence of results of the ACA on different bath truncations in a variety of parameter ranges of the model. Finally we combine the ACA with the local approximation to treat finite Hubbard rings.

## II. THEORETICAL FOUNDATIONS

### A. Reduced density-matrix functional theory

The main quantity of interest for an interacting many-particle problem is the grand potential given as

$$\Omega_{\beta,\mu}(\hat{h} + \hat{W}) = -\frac{1}{\beta} \ln \left[ \text{Tr} \left\{ e^{-\beta(\hat{h} + \hat{W} - \mu \hat{N})} \right\} \right], \quad (1)$$

where  $\beta = 1/(k_B T)$ ,  $k_B$  is the Boltzmann constant,  $T$  is the temperature and  $\mu$  is the chemical potential. In an orthonormal one-particle basis set, the non-interacting part  $\hat{h}$  of the Hamiltonian can be written as

$$\hat{h} = \sum_{a,b} h_{a,b} \hat{c}_a^\dagger \hat{c}_b, \quad (2)$$

the number operator  $\hat{N}$  as

$$\hat{N} = \sum_a \hat{c}_a^\dagger \hat{c}_a, \quad (3)$$

and the general two-particle interaction Hamiltonian  $\hat{W}$  as

$$\hat{W} = \frac{1}{2} \sum_{a,b,c,d} U_{a,b,d,c} \hat{c}_a^\dagger \hat{c}_b^\dagger \hat{c}_c \hat{c}_d \quad (4)$$

using the creation and annihilation operators  $\hat{c}_a^\dagger$  and  $\hat{c}_a$ .

The one-particle reduced density matrix  $\rho_{b,a}$  of an ensemble of normalized fermionic many-particle wave functions  $|\Psi_i\rangle$  with probabilities  $P_i$  ( $0 \leq P_i \leq 1$ ) is defined as

$$\rho_{b,a} = \sum_i P_i \langle \Psi_i | \hat{c}_a^\dagger \hat{c}_b | \Psi_i \rangle. \quad (5)$$

All hermitian matrices that can be generated by Eq. (5) from an ensemble of normalized fermionic many-particle wave functions  $|\Psi_i\rangle$  with probabilities  $P_i$  are called ensemble representable. Coleman<sup>35</sup> has shown that ensemble representability is equivalent to the property, that the eigenvalues of the one-particle reduced density matrix, called occupations by Loewdin<sup>36</sup>, are between zero and one. This is equivalent to the condition, that  $\boldsymbol{\rho}$  and  $\mathbf{1} - \boldsymbol{\rho}$  are positive semi-definite, in short  $\mathbf{0} \leq \boldsymbol{\rho} \leq \mathbf{1}$ .

Within reduced density-matrix functional theory<sup>1-3</sup> (rDMFT) the grand potential can be written as

$$\Omega_{\beta,\mu}(\hat{h} + \hat{W}) = \min_{\boldsymbol{\rho}, \mathbf{0} \leq \boldsymbol{\rho} \leq \mathbf{1}} \left\{ \text{Tr}[\boldsymbol{\rho}(\mathbf{h} - \mu \mathbf{1})] + F_\beta^{\hat{W}}[\boldsymbol{\rho}] \right\} \quad (6)$$

where the minimization is performed over all ensemble-representable one-particle reduced density matrices  $\boldsymbol{\rho}$ .

Knowing the one-particle density matrix, expectation values of one-particle operators are easily accessible. The relation of interaction energy which contains two-particle operators to the one-particle density matrix is less clear. It is encoded in the density-matrix functional  $F_\beta^{\hat{W}}[\boldsymbol{\rho}]$  in Eq. (6).

This functional is an universal functional of the one-particle reduced density matrix in the sense that it does not depend on the external one-particle potential of the system<sup>1</sup>.

Levy<sup>2</sup> and Valone<sup>37</sup> have shown that the density-matrix functional can be obtained from a constrained minimization over an ensemble of orthonormal fermionic many-particle wave functions  $|\Psi_i\rangle$  and ensemble probabilities  $P_i$  with  $0 \leq P_i \leq 1$  and  $\sum_i P_i = 1$  as

$$F_\beta^{\hat{W}}[\boldsymbol{\rho}] = \min_{\{P_i, |\Psi_i\rangle\} \rightarrow \boldsymbol{\rho}} \left[ \sum_i P_i \langle \Psi_i | \hat{W} | \Psi_i \rangle + \frac{1}{\beta} \sum_i P_i \ln(P_i) \right]. \quad (7)$$

Here we denote with  $\{P_i, |\Psi_i\rangle\} \rightarrow \boldsymbol{\rho}$  the set of ensembles with a given one-particle reduced density matrix  $\boldsymbol{\rho}$  according to Eq. (5).

In practical calculations it is often advantageous to work with a thermodynamic ensemble with fixed total particle number. Similarly to the grand potential in Eq. (6) we can express the Helmholtz potential  $A_{\beta,N}(\hat{h} + \hat{W})$  for the fixed particle number  $N$  and inverse temperature  $\beta$  as<sup>2,3,38</sup>

$$A_{\beta,N}(\hat{h} + \hat{W}) = \min_{\boldsymbol{\rho}, \mathbf{0} \leq \boldsymbol{\rho} \leq \mathbf{1}, \text{Tr}[\boldsymbol{\rho}] = N} \left\{ \text{Tr}[\boldsymbol{\rho} \mathbf{h}] + F_\beta^{\hat{W}}[\boldsymbol{\rho}] \right\} \quad (8)$$

### B. Local approximation

Currently, an exact calculation of the density-matrix functional using the constrained minimization in Eq. (7) for a general problem is only possible for very small systems of up to 28 spin-orbitals. In order to divide the extended many-particle problem into impurity problems the local approximations<sup>33</sup> of the interaction and density-matrix functional have been introduced.

In the local approximation of the interaction one selects disjoint sets  $C_R$  of one-particle basis states. Then the interaction  $\hat{W}$  is approximated by a sum of local terms  $\hat{W}_R$ , that act only within a local cluster  $C_R$  of one-particle basis states, i.e.

$$\hat{W} \approx \sum_R \hat{W}_R \quad (9)$$

$$\hat{W}_R = \frac{1}{2} \sum_{a,b,c,d \in C_R} U_{a,b,d,c} \hat{c}_a^\dagger \hat{c}_b^\dagger \hat{c}_c \hat{c}_d. \quad (10)$$

Interactions between clusters are neglected. This approximation defines the multi-band Hubbard model<sup>39-44</sup>. The plethora of investigations on the Hubbard model<sup>45</sup> have shown that local interactions can describe many important correlation effects.

The density-matrix functional with the local approximation for the interaction can be written as

$$F_{\beta}^{\hat{W}}[\rho] \approx F_{\beta}^{\sum_R \hat{W}_R}[\rho]. \quad (11)$$

The second step of the local approximation, i.e. the local approximation of the density-matrix functional itself, approximates the density-matrix functional of a sum of interactions as a sum of density-matrix functionals of individual interactions in the form

$$F_{\beta}^{\sum_R \hat{W}_R}[\rho] \approx \sum_R F_{\beta}^{\hat{W}_R}[\rho]. \quad (12)$$

It should be emphasized, that the one-particle reduced density matrix  $\rho$  in Eq. (12) is still the density matrix of the full one-particle basis of the extended system. It has been shown<sup>33</sup> that the sum of local density-matrix functionals is a lower bound to the exact density-matrix functional of a sum of local interactions, i.e.

$$F_{\beta}^{\sum_R \hat{W}_R}[\rho] \geq \sum_R F_{\beta}^{\hat{W}_R}[\rho]. \quad (13)$$

Investigations of small Hubbard chains with the exact density-matrix functional within the local approximation have been performed<sup>33</sup>.

For most parametrized approximate density-matrix functionals, like the Hartree-Fock approximation, the Müller functional<sup>46</sup> and related functionals<sup>18,22,23,47,48</sup> the local approximation of the density-matrix functional Eq. (12) does not introduce further deviations after the local approximation of the interaction Eq. (9).

### C. Adaptive cluster approximation

#### 1. Truncation of non-interacting basis states

After employing the local approximation we are left with a set of impurity problems. For each impurity problem, we need to evaluate the reduced density-matrix functional  $F_{\beta}^{\hat{W}_R}[\rho]$ . Here, the one-particle reduced density matrix  $\rho$  includes all one-particle basis states of the system, so that calculating the density-matrix functional  $F_{\beta}^{\hat{W}_R}[\rho]$  by Eq. (7) still scales exponentially with the size  $N_{\chi}$  of the one-particle basis.

Thus we need to truncate the cluster size. A judicious choice of the one-particle basis set shall minimize the truncation error.

In order to set the stage, let us consider the limiting case of a density-matrix functional  $F^{\hat{W}_A}[\rho]$ , where the one-particle basis  $C$  can be decomposed into two disjoint subsets,  $C_A$  and  $C_B$ , such that the interaction is limited to the cluster  $C_A$ . Then the interaction Hamiltonian is

$$\hat{W}_A = \frac{1}{2} \sum_{a,b,c,d \in C_A} U_{a,b,d,c} \hat{c}_a^{\dagger} \hat{c}_b^{\dagger} \hat{c}_c \hat{c}_d. \quad (14)$$

For a density matrix that is block-diagonal with respect to  $C_A$  and  $C_B$ , i.e.

$$\rho = \begin{pmatrix} \rho_{AA} & \mathbf{0} \\ \mathbf{0} & \rho_{BB} \end{pmatrix}, \quad (15)$$

the density-matrix functional is independent of the block  $\rho_{BB}$  and can be calculated considering  $C_A$  alone,

$$F_{\beta}^{\hat{W}_A}[\rho] = F_{\beta}^{\hat{W}_A}[\rho_{AA}]. \quad (16)$$

Therefore we attempt to bring the density matrix to a nearly block-diagonal form before truncating it. The transformation will depend on the one-particle density matrix.

To simplify the notation for the derivation of the method, we assume that we have an ordered set of  $N_{\chi}$  one-particle basis states of which the first  $N_A$  states interact via the interaction Hamiltonian  $\hat{W}_R$ . For the truncation of the non-interacting states in the cluster approximation, we define the linear mapping  $T_N^{\dagger} \rho T_N$ . It is defined to give the matrix consisting of the first  $N$  rows and  $N$  columns of the matrix  $\rho$ . The truncated density matrix  $\rho_{T_N} \in \mathbb{C}^{N \times N}$  is then

$$\rho_{T_N} = T_N^{\dagger} \rho T_N = \begin{pmatrix} \rho_{1,1} & \dots & \rho_{1,N} \\ \vdots & \ddots & \vdots \\ \rho_{N,1} & \dots & \rho_{N,N} \end{pmatrix}. \quad (17)$$

A cluster approximation of the density-matrix functional can be written as

$$F_{\beta}^{\hat{W}_A}[\rho] \approx F_{\beta}^{\hat{W}_A}[T_N^{\dagger} \rho T_N]. \quad (18)$$

With the cluster approximation, the density-matrix functional has to be calculated for a system with only  $N$  one-particle basis states, instead of the original  $N_{\chi}$  states.

In order to judge the quality of the transformation we introduce the discarded weight which measures the deviation from the block-diagonal form. The discarded weight  $\sigma_N(\rho)$  is defined as the sum of the absolute values of density matrix elements coupling the neglected and remaining basis states:

$$\sigma_N(\rho) = \sum_{i=N+1}^{N_{\chi}} \sum_{j=1}^N |\rho_{i,j}|. \quad (19)$$

A block-diagonal density matrix as Eq. (15) has a vanishing discarded weight  $\sigma_{|C_A|}(\rho) = 0$ . When the discarded weight vanishes, the cluster approximation becomes exact.

#### 2. Transformation of one-particle basis

In the following, we present a systematic way to perform the cluster approximation. Before the truncation we perform a unitary transformation of the bath states. Because the transformation depends directly on the given

one-particle density matrix, we named it the *adaptive cluster approximation* (ACA).

We write the one-particle reduced density matrix  $\rho$  in block-form,

$$\rho = \begin{pmatrix} \rho_{AA} & \rho_{AB} \\ \rho_{AB}^\dagger & \rho_{BB} \end{pmatrix}, \quad (20)$$

where  $\rho_{AA} \in \mathbb{C}^{N_A \times N_A}$  is the density matrix of the interacting one-particle states,  $\rho_{BB} \in \mathbb{C}^{(N_\chi - N_A) \times (N_\chi - N_A)}$  is the bath density matrix and  $\rho_{AB} \in \mathbb{C}^{N_A \times (N_\chi - N_A)}$  couples interacting and non-interacting states.

The value of the density-matrix functional Eq. (7) is invariant under a unitary transformation  $U$  of the one-particle basis. We exploit this freedom to form an inner bath, which captures the main influence of the environment. We choose the unitary transformation such that the impurity orbitals remain unchanged. This transformation has the block-diagonal form

$$U = \begin{pmatrix} \mathbf{1}_{N_A} & \mathbf{0} \\ \mathbf{0} & U_B \end{pmatrix} \quad (21)$$

where  $\mathbf{1}_{N_A}$  is a  $N_A$  by  $N_A$  unity matrix acting on the impurity orbitals, while  $U_B$  is a  $(N_\chi - N_A)$  by  $(N_\chi - N_A)$  unitary matrix acting on the bath orbitals.

This transformation yields the transformed density matrix as

$$\tilde{\rho} = U^\dagger \rho U = \begin{pmatrix} \rho_{AA} & \rho_{AB} U_B \\ U_B^\dagger \rho_{AB}^\dagger & U_B^\dagger \rho_{BB} U_B \end{pmatrix}. \quad (22)$$

The density-matrix functional has the property

$$F_\beta^{\hat{W}_A}[\rho] = F_\beta^{\hat{W}_A}[U^\dagger \rho U]. \quad (23)$$

The freedom of choice for the unitary transformation  $U_B$  of the bath states is exploited to bring the density matrix into the form of a band matrix, i.e.

$$\tilde{\rho} = U^\dagger \rho U \quad (24)$$

$$= \begin{pmatrix} \rho_{AA} & \tilde{\rho}_{AB_1} & \mathbf{0} & \dots \\ \tilde{\rho}_{AB_1}^\dagger & \tilde{\rho}_{B_1 B_1} & \tilde{\rho}_{B_1 B_2} & \mathbf{0} & \dots \\ \mathbf{0} & \tilde{\rho}_{B_1 B_2}^\dagger & \tilde{\rho}_{B_2 B_2} & \tilde{\rho}_{B_2 B_3} & \mathbf{0} & \dots \\ \vdots & \mathbf{0} & \tilde{\rho}_{B_2 B_3}^\dagger & \tilde{\rho}_{B_3 B_3} & \tilde{\rho}_{B_3 B_4} & \ddots \\ & \vdots & \mathbf{0} & \tilde{\rho}_{B_3 B_4}^\dagger & \tilde{\rho}_{B_4 B_4} & \ddots \\ & & \vdots & \ddots & \ddots & \ddots \end{pmatrix} \quad (25)$$

In appendix A, we introduce a practical construction scheme. Furthermore, we show that the minimal possible bandwidth for a general density matrix is given by the number of interacting orbitals  $N_A$ . The construction scheme proposed in this paper reaches this limit.

Eq. 25 creates subsets of bath orbitals, which are arranged in a hierarchical order. The one-particle basis states that couple directly to the interacting impurity will be called the first-level effective bath or  $B_1$ . The first-level effective bath  $B_1$  has  $N_{B_1}$  states. The coupling is due to  $\tilde{\rho}_{AB_1}$ .

The higher-level effective baths are constructed analogously. The  $n$ -th level effective bath  $B_n$  couples directly only to the next lower-level bath  $B_{n-1}$  and to the next higher-level bath  $B_{n+1}$ . It contains  $N_{B_n}$  states. The density matrix of this bath is  $\tilde{\rho}_{B_n B_n}$ . The matrix elements coupling the  $n$ -th level effective bath  $B_n$  to the next higher-level bath is  $\tilde{\rho}_{B_n B_{n+1}}$  and its transpose.

In appendix A we show that each effective bath has a basis set of equal or smaller size than the next lower level, i.e.  $N_A \geq N_{B_1} \geq N_{B_2} \geq \dots$

Truncation of the transformed density matrix  $\tilde{\rho}$  of (25) beyond the  $M$ -th level bath  $B_M$  defines the adaptive cluster approximation ACA(M). The ACA(M) replaces the density-matrix functional  $F_\beta^{\hat{W}_A}[\rho]$  by

$$F_{\beta, \text{ACA}(M)}^{\hat{W}_A}[\rho] = F_\beta^{\hat{W}_A} \left[ T_{N_M}^\dagger \tilde{\rho} T_{N_M} \right] \quad (26)$$

where  $\tilde{\rho} = U^\dagger \rho U$  is the transformed density matrix given by Eq. (25). The size  $N_M$  of the one-particle basis treated explicitly in the ACA(M) is

$$N_M = N_A + \sum_{i=1}^M N_{B_i} \leq (M+1)N_A. \quad (27)$$

### 3. Sensitivity of the density-matrix functional

The sensitivity of the density-matrix functional to a truncation of the one-particle basis, that is the difference  $F^{\hat{W}_A}[\rho] - F^{\hat{W}_A}[T_N^\dagger \rho T_N]$ , can be related to the derivatives of the density-matrix functional with respect to the elements of the density matrix by

$$F^{\hat{W}_A}[\rho] - F^{\hat{W}_A}[T_N^\dagger \rho T_N] \quad (28)$$

$$= \sum_{\alpha > N \vee \beta > N} \int_0^1 d\lambda \frac{\partial F^{\hat{W}_A}[\rho_\lambda]}{\partial \rho_{\lambda, \alpha\beta}} \quad (29)$$

$$\approx \frac{1}{2} \sum_{\alpha > N \vee \beta > N} \left( \frac{\partial F^{\hat{W}_A}[\rho]}{\partial \rho_{\alpha\beta}} + \frac{\partial F^{\hat{W}_A}[T_N^\dagger \rho T_N]}{\partial \rho_{\alpha\beta}} \right) \rho_{\alpha\beta} \quad (30)$$

with  $\rho_\lambda = \lambda \rho + (1-\lambda) T_N^\dagger \rho T_N$  and  $N \geq N_A$ . This means that the error introduced by the truncation is roughly proportional to a sum over the truncated density matrix elements weighted with the corresponding derivative of the density-matrix functional.

In the following we will use this estimate to explore the workings of the adaptive cluster approximation described in the previous section.

We choose a 3-by-3 site half-filled Hubbard cluster on a square lattice with nearest-neighbor hopping and  $U/t = 5$ , i.e.

$$\hat{H}_{\text{cluster}} = -t \sum_{\langle i,j \rangle} \sum_{\sigma} \hat{c}_{i,\sigma}^\dagger \hat{c}_{j,\sigma} + U \sum_{i=1}^N \hat{n}_{i\uparrow} \hat{n}_{i\downarrow}. \quad (31)$$

From the ground-state wave function we obtain the exact one-particle reduced density matrix  $\rho_0$  for zero temperature.

We then apply the local approximation of the density-matrix functional Eq. (12) by restricting the interaction to the central site  $\hat{W}_{\text{center}} = U\hat{n}_{\text{center}\uparrow}\hat{n}_{\text{center}\downarrow}$ . That is, we investigate the properties of the density-matrix functional  $F^{\hat{W}_{\text{center}}}[\rho]$ .

Now we compare the value and derivatives of the density-matrix functional in the local approximation for two density matrices, namely the exact ground-state density matrix  $\rho_0$  and the transformed density matrix  $\tilde{\rho} = U^\dagger \rho_0 U$  defined by Eq. (25). While the values of the density-matrix functionals for the two density matrices  $\rho_0$  and  $\tilde{\rho}$  are equal by construction, their derivatives  $D_{0,\alpha\beta}$  and  $\tilde{D}_{\alpha\beta}$  are different,

$$D_{0,\alpha\beta} = \frac{\partial F^{\hat{W}_{\text{center}}}[\rho_0]}{\partial \rho_{0,\alpha\beta}} \quad (32)$$

$$\tilde{D}_{\alpha\beta} = \frac{\partial F^{\hat{W}_{\text{center}}}[\tilde{\rho}]}{\partial \tilde{\rho}_{\alpha\beta}}. \quad (33)$$

A histogram of the absolute values of the derivatives is shown in Fig. 1. The transformation to a banded density matrix causes a drastic reduction of the number of derivatives with small absolute values and a general shift towards higher absolute values. In other words the matrix of derivatives  $\tilde{D}_{\alpha\beta}$  is much sparser for the transformed one-particle basis than for the original one  $D_{0,\alpha\beta}$ .

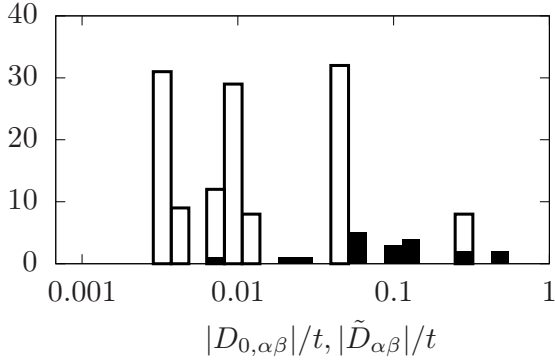


FIG. 1. Histogram of the absolute values of the derivatives  $D_{0,\alpha\beta}$  and  $\tilde{D}_{\alpha\beta}$  defined in Eq. (32) of the local density-matrix functional  $F^{\hat{W}_{\text{center}}}$  with respect to the elements of the reduced density matrix. The derivatives  $D_{0,\alpha\beta}$  with respect to the untransformed one-particle density matrix  $\rho_0$  (open boxes) and the corresponding values  $\tilde{D}_{\alpha\beta}$  for the transformed one-particle basis  $\tilde{\rho} = U^\dagger \rho_0 U$  (filled boxes) are shown.  $\rho_0$  is the exact ground-state density matrix of a half-filled 3-by-3 site Hubbard cluster on a two-dimensional square lattice with  $U/t = 5$  described by the Hamiltonian Eq. (31).  $\tilde{\rho} = U^\dagger \rho_0 U$  is the corresponding transformed density matrix and has a form given by Eq. (25).  $\hat{W}_{\text{center}}$  stands for the interaction on the central site of the cluster.

Fig. 2 shows the dependence of the derivatives

$\tilde{D}_{1\uparrow,\beta\sigma} = \partial F^{\hat{W}_{\text{center}}}[\tilde{\rho}]/\partial \tilde{\rho}_{1\uparrow,\beta\sigma}$  on the bath level  $\beta$  and spin  $\sigma$  of the effective bath states. The rapid monotonic decrease of the derivatives with an increasing level of the effective bath states shows the improved locality of the density-matrix functional in the transformed basis.

As discussed in Eq. (30), the error introduced by a truncation of the one-particle basis is determined by two factors: (1) It is proportional to the derivatives of the density-matrix functional with respect to the neglected density matrix elements. The transformation to a banded density matrix in the ACA improves the locality and decreases the magnitude of the derivatives of the density-matrix functional in the transformed basis. (2) It is proportional to the magnitude of the discarded density matrix elements. Due to the banded form, only few elements can contribute, namely only the density matrix elements coupling the impurity with the first level bath or density matrix elements between the  $n$ -th level and  $n+1$ -th level bath.

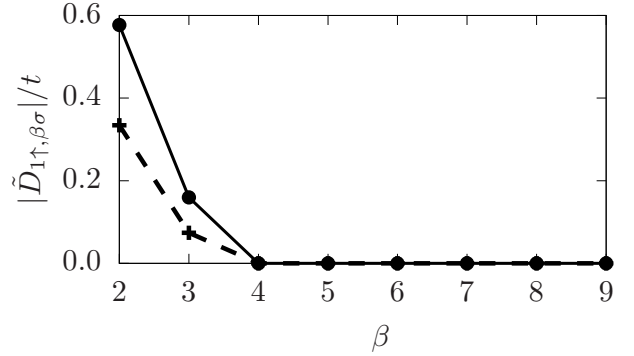


FIG. 2. Dependence of the absolute value of the derivatives  $\tilde{D}_{1\uparrow,\beta\sigma} = \partial F^{\hat{W}_{\text{center}}}[\tilde{\rho}]/\partial \tilde{\rho}_{1\uparrow,\beta\sigma}$  of the local density-matrix functional  $F^{\hat{W}_{\text{center}}}[\tilde{\rho}]$  with respect to the elements of the transformed reduced density matrix on the level  $\beta$  of the effective bath states from the interacting states. The solid line with circles represents results for  $\sigma = \uparrow$  and the dashed line with crosses for  $\sigma = \downarrow$ .  $\rho_0$  is the exact ground-state density matrix of a half-filled 3-by-3 site Hubbard cluster on a two-dimensional square lattice with  $U/t = 5$  described by the Hamiltonian Eq. (31).  $\tilde{\rho} = U^\dagger \rho_0 U$  is the corresponding transformed density matrix given by Eq. (25).  $\hat{W}_{\text{center}}$  stands for the interaction on the central site of the cluster.

#### 4. Relation to existing methods

Methods that employ truncations of one-particle basis sets are omnipresent in the field of quantum chemistry and solid state physics.

The transformation of the one-particle reduced density matrix to a banded matrix within the ACA can be seen as a transformation to a quasi one-dimensional system.

Unitary transformations of the one-particle basis to create a quasi one-dimensional system have been used



to transform impurity problems with arbitrary bath geometries so that they can be treated with DMRG and related methods<sup>49,50</sup>. Unitary transformations of the bath in impurity problems have also been used to express the ground state with a small number of Slater determinants<sup>51,52</sup> or to set up a smaller variationally optimized effective model<sup>53</sup>.

These methods bring the one-particle Hamiltonian rather than the reduced density matrix to a specific shape and are limited to impurity problems. However the local approximation of the interaction and density-matrix functional allow the application of the ACA to general lattice models.

In context of rDMFT a similar approach has already been used within the two-level approximation<sup>14,34</sup> by Töws et al. for the single-impurity Anderson<sup>54</sup> model.

Töws et al. derived the analytical dependence of the density-matrix functional with respect to the density matrix for a simple Anderson problem, i.e. an impurity site and one bath site. To apply this analytical form to more general single-impurity Anderson models, they introduced a unitary transformation of the bath states, so that only two of the transformed bath states have finite density matrix elements with the impurity site. All other bath states have been neglected in the evaluation of the density-matrix functional.

This transformation, although constructed in a different way, is equivalent to the single transformation step Eq. (A6) in the ACA in the case of two interacting spin-orbitals ( $N_A = 2$ ).

Töws et al. used the exact density-matrix functional for the effective two-site problem (impurity site and first-level effective bath site) in case of a non-spin-polarized density matrix<sup>34</sup>, but employed additional approximations for the spin-polarized case<sup>14</sup>. In contrast we calculate the density-matrix functional for the truncated density matrix on the fly via a constrained optimization scheme without additional systematic approximations.

The ACA(M) can be seen as an extension of two-level approximation to an arbitrary number of effective bath states/levels, arbitrary impurity sizes and multi-band interactions.

### 5. Exact limits

The adaptive cluster approximation is exact in the non-interacting limit, because the density-matrix functional vanishes in this case.

For a single-site impurity ( $N_A = 2$ ) the ACA with one effective bath site ( $M = 1$ ) inherits the exact limits from the two-level approximation, that have been proven by Töws et al.<sup>34</sup>: It becomes exact for a single-impurity Anderson<sup>54</sup> model in the limit of a vanishing bath bandwidth and in the limit of widely separated bath levels.

Furthermore if the discarded weight  $\sigma_{N_A+N_B}(\tilde{\rho})$  vanishes for a given number of effective bath states  $N_B$ , then the ACA(M) is exact in this case. Then the transformed

density matrix  $\tilde{\rho} = U^\dagger \rho U$  is in a block-diagonal form with one block of the size  $N_A + N_B$  and one with the remaining  $N_\chi - N_A - N_B$  states.

In Appendix B we prove that if the eigenvalue spectrum of the bath-density matrix  $\rho_{BB}$  in Eq. (20) consist of  $N$  distinct values with a  $n_j$ -fold degeneracy each, there is a number of bath states  $N_B \leq \sum_{j=1}^N \min(n_j, N_A)$  for which the discarded weight  $\sigma_{N_A+N_B}(\tilde{\rho})$  vanishes.

### D. Correction using parametrized functionals

The minimization of the grand potential given in Eq. (6) or the Helmholtz potential in Eq. (8) with the adaptive cluster approximation can produce density matrices with a discarded weight  $\sigma_{N_A+\sum_{i=1}^M N_{B_i}}(\tilde{\rho})$  that is much larger than that for the transformed exact ground-state density matrix.

The reason is, that the truncated off-diagonal density matrix elements  $\tilde{\rho}_{AB_1}$  or  $\tilde{\rho}_{B_n B_{n+1}}$  do not influence the density-matrix functional within the ACA. As a consequence they can become much larger than in the exact solution, if this reduces the one-particle energy in Eq. (6). Our applications to model systems indicate that this becomes relevant only at very low truncation levels.

In order to cope with this problem, we introduce the corrected density-matrix functional, defined by

$$F_{\beta, cACA(M)}^{\tilde{W}}[\rho] = F_{\beta, ACA(M)}^{\tilde{W}}[\rho] + \Delta F_{\beta, \approx}^{\tilde{W}}[\rho], \quad (34)$$

$$\Delta F_{\beta, \approx}^{\tilde{W}}[\rho] = F_{\beta, \approx}^{\tilde{W}}[\tilde{\rho}] - F_{\beta, \approx}^{\tilde{W}}[T_{N_M}^\dagger \tilde{\rho} T_{N_M}], \quad (35)$$

with  $\tilde{\rho} = U^\dagger \rho U$  given by Eq. (25) and  $N_M = N_A + \sum_{i=1}^M N_{B_i}$ . We name this the corrected ACA (cACA). The correction  $\Delta F_{\beta, \approx}^{\tilde{W}}[\rho]$  is expressed with the help of a density-matrix functional  $F_{\beta, \approx}^{\tilde{W}}[\rho]$ , that should be easy to evaluate. Suitable are for example parametrized approximations in an analytical form.

In this work we choose the Müller density-matrix functional<sup>46</sup> as the correction functional  $F_{\beta, \approx}^{\tilde{W}}[\rho]$  in Eq. (35). The Müller functional is defined by the analytical expression

$$F_{\beta, \approx}^{\tilde{W}}[\rho] = \frac{1}{2} \sum_{\alpha\beta\gamma\delta} U_{\alpha\beta\gamma\delta} \rho_{\delta\alpha} \rho_{\gamma\beta} - \frac{1}{2} \sum_{m,n} (f_m f_n)^{\frac{1}{2}} \sum_{\alpha\beta\gamma\delta} U_{\alpha\beta\delta\gamma} \phi_{m,\gamma} \phi_{m,\alpha}^* \phi_{n,\delta} \phi_{n,\beta}^*, \quad (36)$$

where  $f_n$  denote the occupations,  $\phi_{n,\alpha}$  the matrix of natural orbitals and  $U_{\alpha\beta\delta\gamma}$  interaction matrix elements.

The choice of an approximate density-matrix functional  $F_{\beta, \approx}^{\tilde{W}}$  is limited by the requirement that it should be invariant with respect to unitary transformations of the one-particle basis as in Eq. (23). The invariance with respect to a unitary transformation guarantees that the correction vanishes in cases where the discarded weight

is zero, that is when a complete decoupling of the density matrix is possible.

Furthermore the derivatives of  $F_{\beta,\approx}^{\hat{W}}[\tilde{\rho}]$  with respect to the off-diagonal sub-matrices  $\tilde{\rho}_{AB_1}$  and  $\tilde{\rho}_{B_n B_{n+1}}$  in Eq. (25) should not vanish by construction. For example this condition is not fulfilled for the Hartree-Fock approximation, because in this approximation the value of the functional,

$$F_{\text{HF}}^{\hat{W}}[\rho] = \frac{1}{2} \sum_{\alpha\beta\gamma\delta} U_{\alpha\beta\gamma\delta} (\rho_{\delta\alpha}\rho_{\gamma\beta} - \rho_{\gamma\alpha}\rho_{\delta\beta}), \quad (37)$$

is independent of density matrix elements of non-interacting states.

### III. NUMERICAL METHODS

#### A. Exact ground-state energies and many-particle wave functions

To benchmark the performance of the adaptive cluster approximation for a single-impurity Anderson model, we have calculated the exact ground-state energy and many-particle wave function for this system at zero temperature with an exact diagonalization algorithm based on the Jacobi-Davidson method implemented in Jadamilu<sup>55</sup>.

The exact ground-state energy, one-particle energy, interaction energy and nearest-neighbor density matrix elements for the half-filled Hubbard ring at zero temperature were calculated by solving the Bethe ansatz equations numerically<sup>56,57</sup>.

#### B. Minimization over the one-particle reduced density matrix

The minimization over the ensemble-representable one-particle reduced density matrix in Eq. (6) respectively Eq. (8) is performed using a Car-Parrinello-like<sup>58</sup> constrained minimization. For that purpose the density matrix is written in its spectral representation as

$$\rho = \sum_{i=1}^{N_x} f_i \phi_i^\dagger \phi_i \quad (38)$$

with the occupations  $f_i \in \mathbb{R}$  and the eigenvectors  $\phi_i \in \mathbb{C}^{N_x}$ , which are called natural orbitals<sup>36</sup>. The ensemble representability of the density matrix requires the occupations to be between 0 and 1. This condition is satisfied by expressing the occupations as  $f_i = [1 - \cos(x_i)]/2$  with unconstrained variables  $x_i$ . Using the set of  $x_i$  and the natural orbitals as dynamical quantities, a fictitious Lagrangian for the calculation of the Helmholtz potential

can be set up in the form

$$\begin{aligned} \mathcal{L} = & \frac{1}{2} \sum_{i=1}^{N_x} m_x \dot{x}_i^2 + \sum_{i=1}^{N_x} f(x_i) m_\phi |\dot{\phi}_i|^2 \\ & - \text{Tr}[\rho \mathbf{h}] - F^{\hat{W}}[\rho] + \mu (\text{Tr}[\rho] - N) \\ & + \sum_{i,j} \Lambda_{i,j} (\phi_i^* \cdot \phi_j - \delta_{i,j}) \end{aligned} \quad (39)$$

where  $\rho$  is given in terms of the occupations and natural orbitals by Eq. (38).  $\mu$  and  $\Lambda_{i,j}$  are Lagrange multipliers for the particle number constraint and orthonormality.

Starting from a random initial guess the Euler-Lagrange equations are integrated using the Verlet algorithm<sup>59</sup>. The particle number constraint and the orthonormality constraint of the natural orbitals are enforced in every time step of the integration with the help of the corresponding Lagrange multipliers<sup>60</sup>.

A minimum of the potential energy

$$\text{Tr}[\rho \mathbf{h}] + F^{\hat{W}}[\rho] \quad (40)$$

of the fictitious Lagrangian with respect to the constraints is obtained by including an additional friction term.

The convergence criterion for the numerical minimization of the total energy given by Eq. (8) is chosen as  $10^{-4}t$ , where  $t$  is the hopping parameter. For the investigation of the bandwidth dependence of the single-impurity Anderson model, where the energy scale is set by the hybridization parameter  $V$ , we choose  $10^{-4}V$  as the convergence criterion. The convergence is verified by propagating the Car-Parrinello dynamics without friction for a large number of steps and checking that the energy stays within a window defined by the given convergence criterion.

The search space includes density matrices with broken spin-symmetry and non-collinear density matrices. For the Hubbard rings discussed in section IV B, we restricted the density matrix to be translation symmetric along the ring on the ring and non-spin-polarized.

#### C. Evaluation of the exact density-matrix functional

We explore the performance of the (corrected) adaptive cluster approximation in the zero temperature limit. This allows to reduce the ensemble for non-degenerate ground states to a single many-particle wave function, i.e.  $N_\psi = 1$ . The density-matrix functional simplifies to

$$F_{N_\psi=1}^{\hat{W}}[\rho] = \min_{|\Psi\rangle \rightarrow \rho} \langle \Psi | \hat{W} | \Psi \rangle. \quad (41)$$

To simplify the notation, we omit the subscript  $N_\psi = 1$  in the following. For the models studied here, the precondition that ground states are non-degenerate is fulfilled.

The many-particle wave function is represented as a superposition of Slater determinants with variable coefficients. A complete set of Slater determinants is used in the present study. We use a convergence criterion of  $10^{-5}t$  for all calculations except for the case of the bandwidth dependence of the single-impurity Anderson model, where we have used  $10^{-5}V$ . Details of the constrained search algorithm will be presented elsewhere.

#### IV. BENCHMARK RESULTS

##### A. Single-impurity Anderson model

###### 1. Definition of the model

To investigate the properties of the adaptive cluster approximation, we have chosen the same finite single-impurity Anderson<sup>54</sup> model as in the first publication of the so-called two-level approximation of Töws and Pastor<sup>34</sup>.

It consists of one impurity site with a local density-density interaction and a ring of  $N_{\text{bath}}$  non-interacting bath-sites with nearest-neighbor hopping. Electrons on the impurity site can hop directly to only one of the bath sites.

The Hamiltonian can be divided into three parts:

$$\hat{H} = \hat{H}_{\text{imp}} + \hat{H}_{\text{bath}} + \hat{H}_{\text{hyb}}. \quad (42)$$

The impurity Hamiltonian  $\hat{H}_{\text{imp}}$  contains the impurity on-site energy  $\epsilon_f$  and a local two-particle interaction  $\hat{W} = U\hat{n}_{f,\uparrow}\hat{n}_{f,\downarrow}$  with the interaction parameter  $U$

$$\hat{H}_{\text{imp}} = \sum_{\sigma \in \{\uparrow, \downarrow\}} \epsilon_f \hat{f}_\sigma^\dagger \hat{f}_\sigma + \hat{W}. \quad (43)$$

$\hat{f}_\sigma^\dagger$  ( $\hat{f}_\sigma$ ) denotes the creation (annihilation) operator for an electron in the spin-state  $\sigma \in \{\uparrow, \downarrow\}$  in the impurity orbital. The number operator for the impurity orbital is defined as  $\hat{n}_{f,\sigma} = \hat{f}_\sigma^\dagger \hat{f}_\sigma$ .

The one-particle Hamiltonian of the bath, i.e. the non-interacting ring, has the form

$$\hat{H}_{\text{bath}} = -t \sum_{\langle i,j \rangle} \sum_{\sigma \in \{\uparrow, \downarrow\}} \hat{c}_{i,\sigma}^\dagger \hat{c}_{j,\sigma} + h.c., \quad (44)$$

where  $\hat{c}_{i,\sigma}$  ( $\hat{c}_{i,\sigma}^\dagger$ ) denotes the creation (annihilation) operator for a state at the bath site  $i$  with spin  $\sigma$ .  $\langle i,j \rangle$  restricts the summation to pairs of nearest-neighbor bath sites.

The hybridization Hamiltonian  $\hat{H}_{\text{hyb}}$ , that describes the hopping between impurity and bath, can be written as

$$\hat{H}_{\text{hyb}} = V \sum_{\sigma \in \{\uparrow, \downarrow\}} \left( \hat{f}_\sigma^\dagger \hat{c}_{1,\sigma} + \hat{c}_{1,\sigma}^\dagger \hat{f}_\sigma \right) \quad (45)$$

with the hybridization parameter  $V$ .

The energy eigenvalues of the one-particle Hamiltonian of the non-interacting bath in Eq. (44) are

$$\epsilon_k = -2t \cos\left(\frac{2\pi k}{N_{\text{bath}}}\right), \quad (46)$$

with  $k \in \{0, \dots, N_{\text{bath}} - 1\}$ .

In the Bloch basis that diagonalizes the bath one-particle Hamiltonian the hybridization Hamiltonian can be written as

$$\hat{H}_{\text{hyb}} = \frac{V}{\sqrt{N_{\text{bath}}}} \sum_{k=0}^{N_{\text{bath}}-1} \sum_{\sigma \in \{\uparrow, \downarrow\}} \left( \hat{f}_\sigma^\dagger \hat{c}_{k,\sigma} + \hat{c}_{k,\sigma}^\dagger \hat{f}_\sigma \right). \quad (47)$$

Here  $\hat{c}_{k,\sigma}$  ( $\hat{c}_{k,\sigma}^\dagger$ ) are the creation (annihilation) operators of a state in the Bloch basis with momentum quantum number  $k$  and spin  $\sigma$ . As a consequence this model can equivalently be described as an impurity site coupled to all  $N_{\text{bath}}$  bath sites with on-site-energies of the bath orbitals given by Eq. (46) and a hybridization strength of  $V/\sqrt{N_{\text{bath}}}$ . A comprehensive discussion of the underlying physics of this model has been given by Töws and Pastor<sup>34</sup>.

###### 2. Interaction-strength dependence

In this section we show exact zero-temperature results for the total ground-state energy  $E_0 = \langle \psi_0 | \hat{H} | \psi_0 \rangle$ , interaction energy  $W_0 = \langle \psi_0 | \hat{W} | \psi_0 \rangle$  and impurity occupation  $n_f = \langle \psi_0 | \hat{n}_{f,\uparrow} + \hat{n}_{f,\downarrow} | \psi_0 \rangle$  at half filling, i.e. with  $N_{\text{bath}} + 1$  electrons, and briefly discuss the physical background. We compare these exact results to the (corrected) adaptive cluster approximation to evaluate its performance for this system.

The interaction strength-dependence is investigated in this section, the impurity on-site-energy dependence in appendix C1 and the bandwidth dependence in appendix C2.

*a. Exact results* The influence of the interaction strength  $U/t$  on the exact and the Hartree-Fock ground state is shown in Fig. 3. The parameters were  $N_{\text{bath}} = 11$ ,  $\epsilon_f = 0$ ,  $t > 0$ ,  $V/t = 0.4$  and  $U/t \in [0, 8]$ . The SIAM is half-filled, i.e. the particle number is fixed to  $N_e = N_{\text{bath}} + 1 = 12$ . Consequently the impurity can be occupied by between zero and two electrons, while the bath can contain between 10 and 12 electrons. The energy levels of the bath are given in Eq. (46).

The Fermi level  $\epsilon_{F,\text{bath}}$  of the bath for a particle number  $N_e$  is defined as

$$\epsilon_{F,\text{bath}} = \left. \frac{\partial E_{\text{bath}}(N)}{\partial N} \right|_{N=N_e}, \quad (48)$$

where  $E_{\text{bath}}(N)$  is the energy of the non-interacting bath with  $N$  electrons.



The bath-Fermi level  $\epsilon_{F,\text{bath}}$  for the model under investigation here is given by the one-particle energy of the eleventh and twelfth energy level of the non-interacting bath,

$$\epsilon_{F,\text{bath}} = -2t \cos(2\pi \cdot 3/11) \approx 0.28t > 0. \quad (49)$$

Because the impurity level  $\epsilon_f = 0$  is chosen to lie below the bath-Fermi level  $\epsilon_{F,\text{bath}} > 0$  the impurity is more than half-filled, i.e.  $n_f > 1$ , in the non-interacting limit  $U = 0$ . Due to the finite impurity-bath hybridization the impurity is not completely filled  $n_f < 2$  except for a completely filled bath.

When increasing the interaction strength from  $U = 0$ , electrons are transferred from the impurity to the bath, because the interaction penalizes the double occupation  $\langle \hat{n}_{f,\uparrow} \hat{n}_{f,\downarrow} \rangle$  on the impurity. For small interaction strengths we have the simple quadratic relation  $W \approx U n_f^2/4$  between the interaction energy  $W$  and the impurity occupation. This relation follows directly from the Hartree-Fock approximation of the density-matrix functional for a non-magnetic one-particle reduced density matrix.

For large interaction strengths  $U/t \rightarrow \infty$  the double occupancy on the impurity is completely suppressed and the interaction energy goes to zero. This does not imply that the impurity occupation goes to zero as well. The impurity occupation rather approaches a finite value, namely  $n_f \approx 0.7123$ .

In the large-interaction limit, the impurity occupation  $n_f$  is smaller than one, because the ground state wave function can only include Slater determinants with at most one electron on the impurity. In the large interaction limit, the limiting cases for the hybridization  $V$  are readily obtained: (1) The impurity occupation approaches  $n_f = 1/2$  for large hybridization  $V/t \rightarrow \infty$ . (2) With our choice of the bath-Fermi level with  $\epsilon_f < \epsilon_{F,\text{bath}}$ , the impurity occupation approaches  $n_f = 1$  for weak hybridization  $V/t \rightarrow 0$ .

As anticipated, the spin-unrestricted Hartree-Fock approximation agrees well with the exact result for small interaction strengths and yields an upper bound to the exact ground-state energy. However, as shown in the inset of Fig. 3, the HF solution undergoes a transition to a qualitatively incorrect ground state at  $U \approx t$  with a finite magnetization  $m_f = n_{f,\uparrow} - n_{f,\downarrow}$  on the impurity.

*b. ACA for the exact ground-state density matrix*  
We evaluate the performance of the ACA on two levels: first we investigate its local performance and in a second step we analyze its global properties. For the local performance we investigate the accuracy for a fixed density matrix, namely the exact ground state density matrix  $\rho_0$ . The global properties will be investigated by employing the ACA in a minimization over the full space of one-particle density matrices.

The number of effective basis states  $N_M$ , including the  $N_A$  impurity states, for the lowest  $M$  effective bath levels is given by Eq. (27) as  $N_M = N_A + \sum_{i=1}^M N_{B_i} \leq (M+1)N_A$ . Here  $(M+1)N_A$  is only an upper bound

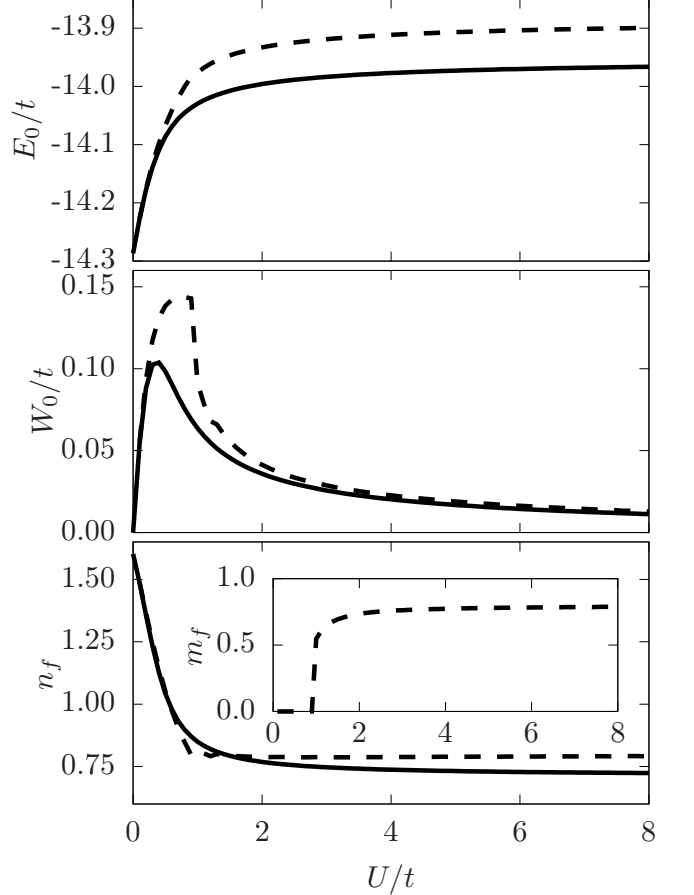


FIG. 3. Ground-state energy  $E_0$ , interaction energy  $W_0$  and impurity occupation  $n_f$  of the exact ground state (solid lines) and the unrestricted Hartree-Fock ground state (dashed lines) of the Hamiltonian defined Eq. (42)-(47) with  $N_{\text{bath}} = 11$ ,  $\epsilon_f = 0$ ,  $t > 0$ ,  $V/t = 0.4$  at half filling. The inset in the third graph shows the magnetic moment  $m_f = n_{f,\uparrow} - n_{f,\downarrow}$  of the impurity within the unrestricted Hartree-Fock approximation.

for  $N_M$ , because the minimal number of effective bath states  $N_{B_i}$  for a bath level  $i$  is equal to the matrix ranks of submatrices  $rk(\rho_{AB_i})$  in Eq. (A1) and  $rk(\tilde{\rho}_{B_i C_i})$  in Eq. (A7).

In practical applications of the ACA, the matrices  $\tilde{\rho}_{AB_i}$  and  $\tilde{\rho}_{B_i C_i}$  will have full rank. Their rank is equal to the number of impurity basis states  $N_A$ . As a consequence, the number  $N_M$  of effective basis states for the lowest  $M$  effective bath levels is  $N_M = (M+1)N_A$ .

For the SIAM investigated here, there are  $N_A = 2$  impurity orbitals. Thus the number  $N_M$  of effective bath sites for a given truncation parameter  $M$  is  $N_M = 2(M+1)$ . Thus, the ACA leads to a much smaller effective system with  $2(M+1)$  basis states instead of the original  $N_A + 2N_{\text{Bath}} = 24$  basis states.

The discarded weight  $\sigma_{2(M+1)}(U^\dagger \rho_0 U)$  for the exact ground-state density matrix  $\rho_0$ , which has been transformed as described in section II C 2, is shown in Fig. 4

for the lowest three truncation levels. In section II C 5, it has been discussed that a spectrum of the bath density matrix with three sets of degenerate eigenvalues implies convergence for truncation at  $M = 3$  bath sites. There is one set of ten small eigenvalues with values below  $4 \cdot 10^{-3}$ . A second set of ten eigenvalues lies close to 1, i.e. between  $1 - 10^{-4}$  and 1. The third, doubly degenerate set lies between the first two sets.

Fig. 4 shows that the discarded weight for a single effective bath site, i.e.  $M = 1$ , is much smaller than that for  $M = 2$ .

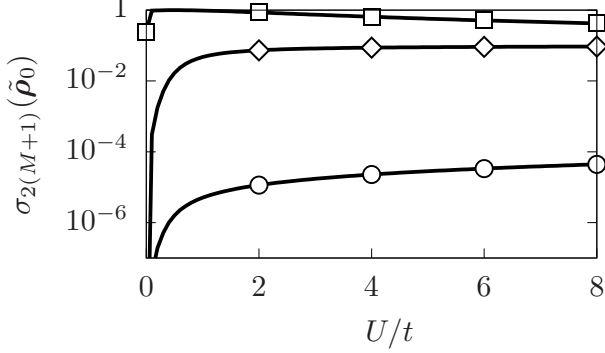


FIG. 4. Discarded weight  $\sigma_{2(M+1)}(\tilde{\rho}_0)$  given by Eq. (19) of the transformed one-particle reduced density matrix  $\tilde{\rho}_0 = \mathbf{U}^\dagger \rho_0 \mathbf{U}$  (see Eq. (25)) of the Hamiltonian defined Eq. (42)-(47) with  $N_{\text{bath}} = 11$ ,  $\epsilon_f = 0$ ,  $t > 0$ ,  $V/t = 0.4$  at half filling. Truncation with  $M = 1$  (solid line with diamonds),  $M = 2$  (solid line with squares) and  $M = 3$  (solid line with circles).

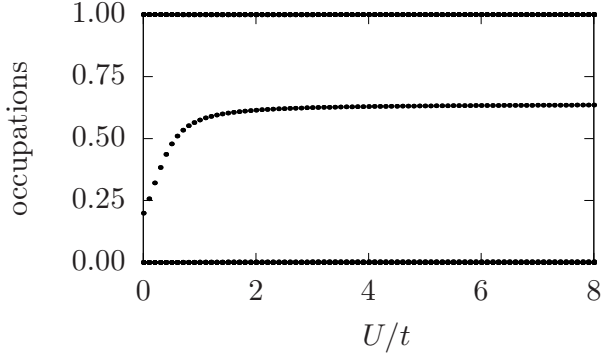


FIG. 5. Eigenvalue spectrum (occupations) of the bath density matrix  $\rho_{BB}$  of the exact ground state of the Hamiltonian defined Eq. (42)-(47) with  $N_{\text{bath}} = 11$ ,  $\epsilon_f = 0$ ,  $t > 0$ ,  $V/t = 0.4$  at half filling.

Fig. 6 shows the deviation of the density-matrix functional obtained with the (corrected) adaptive cluster approximation from the exact functional. Even, the lowest truncation level  $M = 1$ , which is equivalent to the two-level approximation, already performs well for the exact ground-state density matrix.

The two lowest truncation levels,  $M = 1$  and  $M = 2$ ,

produce similar errors. This is due to the fact that the discarded weight  $\sigma_{2(M+1)}(\mathbf{U}^\dagger \rho_0 \mathbf{U})$  for the transformed exact ground-state density matrix for  $M = 2$  is much larger than for  $M = 1$  as shown in Fig. 4. Even though a given finite discarded weight causes a smaller deviation for increasing truncations levels, the large discarded weight for  $M = 2$  compared to  $M = 1$  compensates this.

The correction (Eq. (35)) described in section II D obtained with the Müller functional improves the result for small interaction strengths  $U/t < 2$ . However, for large interactions the correction worsens the results for  $M = 1$  and  $M = 2$ .

The very small discarded weight  $\sigma_{2(M+1)}(\tilde{\rho}_0) \leq 10^{-4}$  for  $M = 3$  shown in Fig. 4 implies that the ACA produces an extremely small error of the density-matrix functional for the exact ground-state density matrix of this system. The deviation introduced by the ACA in this case is far below the convergence criterion for the constrained optimization solver for the density-matrix functional employed in this work. This shows that the density-matrix functional of this model can be approximated very precisely from an effective four-site system instead of the original twelve-site system.

*c. Full minimization over the one-particle reduced density matrix* In the previous section, the accuracy of the ACA for the SIAM has been explored from a local point of view, that is for a specific density matrix. Now we investigate the global properties. They are most relevant, because the main purpose of density-matrix-functional theory is the global optimization of the density matrix in order to obtain the ground state energy and its electronic structure.

In figure 7, the deviations of energies and impurity occupations obtained by the ACA from the exact results are shown as function of interaction strength.

The most important result is that the ACA does not produce the symmetry breaking obtained with the Hartree-Fock approximation. This is true even for the lowest truncation level  $M = 1$ . The ground-state density matrix obtained with the ACA agrees well with the exact one. As a consequence the deviations of the density-matrix functional for the optimized density matrix shown in Fig. 7, are similar to those obtained with the fixed exact density matrix shown in Fig. 6.

Increasing the truncation level from  $M = 1$  to  $M = 2$  reduces the differences significantly. This is in strong contrast to our results with the fixed exact ground-state density matrix shown in Fig. 6, where the accuracy of the density-matrix functional for  $M = 1$  and  $M = 2$  was similar.

The ACA overestimates the impurity occupation  $n_f$ . This is a consequence of the underestimation of the interaction energy, which reduces the electron repulsion on the impurity.

On the one hand, the uncorrected ACA shares many features with the two-level-approximation of Töws et al., notably the large relative error of the interaction energy for large interaction strengths<sup>34</sup>. The Müller-corrected

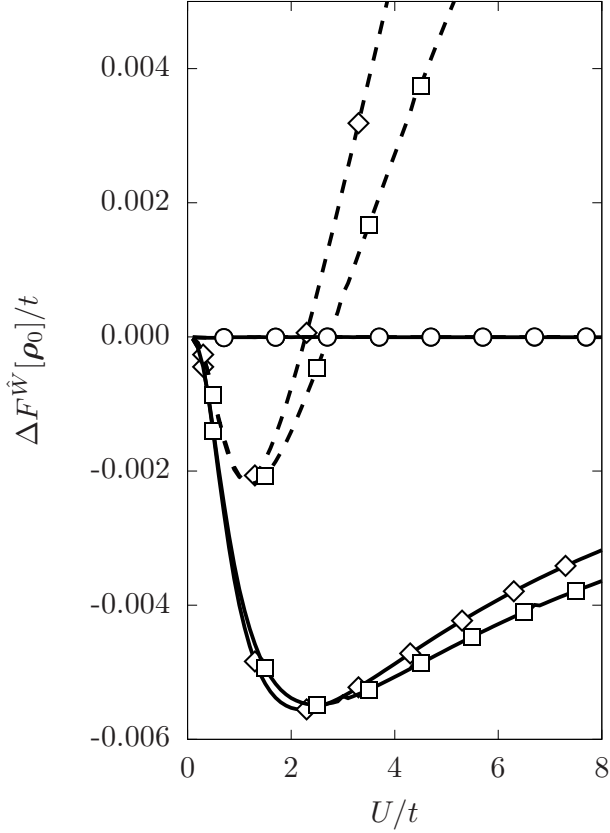


FIG. 6. Difference of the reduced density-matrix functional  $\Delta F^{\hat{W}}[\rho_0] = F_{(c)ACA(M)}^{\hat{W}}[\rho_0] - F^{\hat{W}}[\rho_0]$  in the adaptive cluster approximation to the exact ground-state density-matrix functional for the exact one-particle reduced density matrix  $\rho_0$  of the Hamiltonian defined Eq. (42)-(47) with  $N_{\text{bath}} = 11$ ,  $\epsilon_f = 0$ ,  $t > 0$ ,  $V/t = 0.4$  at half filling. Solid lines: The density-matrix functional in the adaptive cluster approximation given by Eq. (26); Dashed lines: The density matrix in the corrected adaptive cluster approximation (cACA) given by Eq. (34) and Eq. (35). The symbols denote the truncation level:  $M = 1$  with diamonds,  $M = 2$  with squares and  $M = 3$  with circles.

ACA, on the other hand, greatly improves the results for the entire range of interaction strengths. As intended, the Müller correction improves the result by preventing the growth of discarded weight during the density matrix optimization. This explains why the Müller correction works well for optimization, while its performance for a fixed density matrix (see Fig. 6) has been mixed. The reduction of the discarded weight by the correction has been discussed in Sec. IID and it is demonstrated in Fig. 8.

For large interactions, the Müller correction overcorrects the results for interaction energy and impurity occupation, which is a consequence of the well-known<sup>19-21</sup> overcorrelation of Müller's functional. The overcorrelation of Müller's functional is attenuated in the context of the ACA correction, because it does not affect the dom-

inant contributions.

The results for the full minimization over the reduced density matrix for  $M = 3$ , i.e. three effective bath sites, are also shown in Fig. 7. The minimizations for this truncation parameter, that were started from random ensemble  $N$ -representable density matrices, converged to the exact result within the numerical precision of the constrained optimization solver of the density-matrix functional.

In conclusion, the ACA with and without correction describes the interaction-strength dependence of the single-impurity Anderson model very well in the weakly as well as in the strongly interacting regime. Correlation effects are correctly described without unphysical symmetry breaking.

### 3. Impurity on-site-energy dependence and bandwidth dependence

The impurity on-site-energy dependence is investigated in detail in appendix C1. It is shown, that the ACA can properly describe the Kondo regime without an unphysical spin symmetry breaking. The results for the bandwidth dependence in appendix C2 show that the ACA with one effective bath site becomes exact in the limit of a vanishing bath bandwidth  $t \rightarrow 0$  and in the limit of widely separated bath levels  $t \rightarrow \infty$ . This follows from the equivalence of the uncorrected ACA with  $M = 1$  to the two-level approximation<sup>34</sup>.

## B. Hubbard ring

### 1. Definition of the model

In this section, we explore the performance of the ACA in combination with the local approximation of the density-matrix functional, described in sec. IIB. In contrast to the SIAM studied before, we consider now a Hubbard model<sup>39-45</sup> with interactions on all sites. In the local approximation, the density-matrix functional is a sum over all sites, where each site contribution has only one interacting site. We emphasize that there is only one density matrix for the entire system, which experiences the forces from all sites simultaneously.

We apply this scheme to a  $N$ -site Hubbard ring with nearest-neighbor hopping given by the Hamiltonian

$$\hat{H} = \hat{T} + \sum_{i=1}^N \hat{W}_i, \quad (50)$$

where  $\hat{T}$  is the single-particle nearest-neighbor hopping Hamiltonian

$$\hat{T} = -t \sum_{\langle i,j \rangle} \sum_{\sigma} \hat{c}_{i,\sigma}^{\dagger} \hat{c}_{j,\sigma} \quad (51)$$

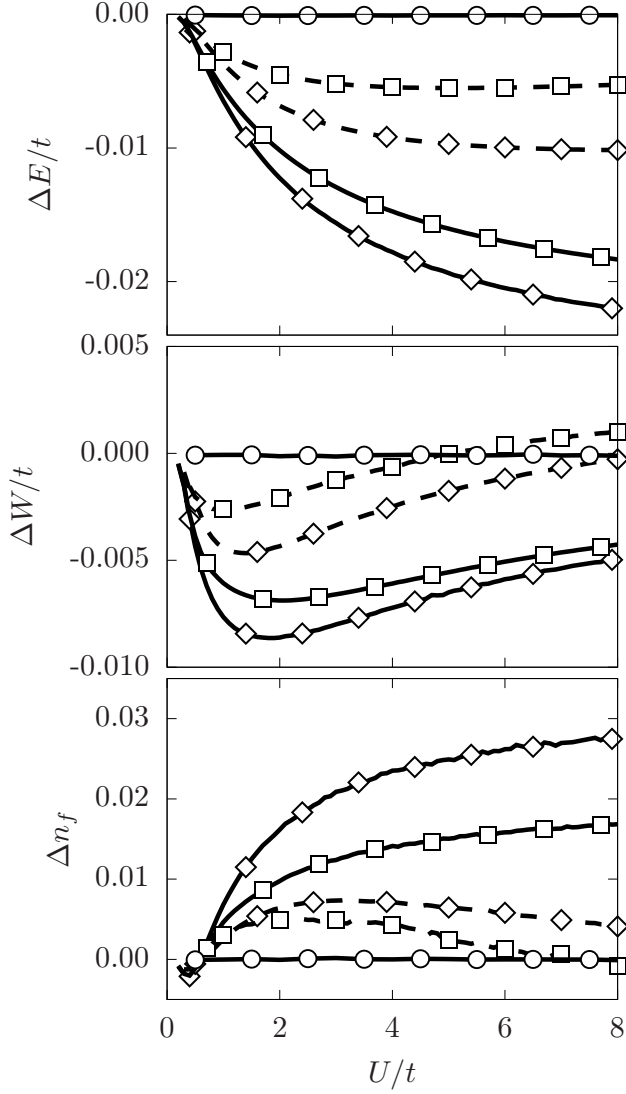


FIG. 7. Deviation of the ground-state energy  $\Delta E = E_{(c)ACA(M)} - E_0$ , interaction energy  $\Delta W = W_{(c)ACA(M)} - W_0$  and impurity occupation  $\Delta n_f = n_{f,(c)ACA(M)} - n_f$  between the ground state within the (corrected) adaptive cluster approximation and the exact ground state. The corresponding exact results are shown in Fig. 3. The Hamiltonian is defined in Eq. (42)-(47) with the parameters  $N_{\text{bath}} = 11$ ,  $\epsilon_f = 0$ ,  $t > 0$ ,  $V/t = 0.4$  and at half filling. Solid lines correspond to the uncorrected ACA and dashed lines to the Müller-corrected ACA results. Truncation with  $M = 1$  (solid line with diamonds),  $M = 2$  (solid line with squares) and  $M = 3$  (solid line with circles). The noise, especially in  $\Delta n_f$ , is due to the finite convergence criterion for the minimization in Eq. (8).

and  $\hat{W}_i$  are the local Hubbard interactions on the  $i$ -th site given as

$$\hat{W}_i = U \hat{n}_{i,\uparrow} \hat{n}_{i,\downarrow}. \quad (52)$$

Exact results for the interaction-strength dependence of this model at half filling calculated with the Bethe

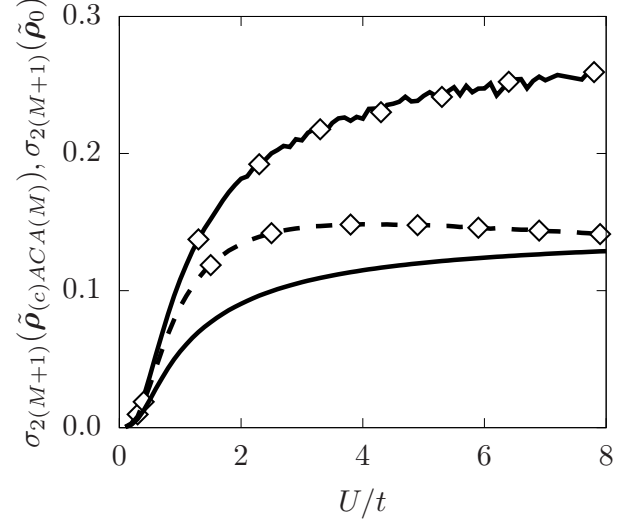


FIG. 8. Discarded weight  $\sigma_{2(M+1)}(\tilde{\rho})$  given by Eq. (19) of the transformed ground state density matrix  $\tilde{\rho}_{(c)ACA(M)}$  within the (corrected) ACA and the transformed exact density matrix  $\tilde{\rho}_0$ . The Hamiltonian is defined in Eq. (42)-(47) with the parameters  $N_{\text{bath}} = 11$ ,  $\epsilon_f = 0$ ,  $t > 0$ ,  $V/t = 0.4$  and at half filling. The ACA-truncation with  $M = 1$  of the transformed exact density matrix  $\tilde{\rho}_0$  (solid line without symbols) is compared the ground state of the uncorrected (solid line with symbols) and corrected (dashed line with symbols) ACA with  $M = 1$ .

ansatz are shown in Fig. 11. In the non-interacting limit, the total energy and nearest-neighbor density matrix elements  $\rho^{NN} = \rho_{i,\sigma,i+1,\sigma}$  are given by

$$E_0/t = -4 - 8 \sum_{i=1}^{(N-2)/4} \cos\left(2\pi \frac{i}{N}\right) \quad (53)$$

$$\rho^{NN} = \frac{E_0}{4Nt}. \quad (54)$$

With increasing interaction strength  $U/t$ , covalent bonding between the sites is suppressed. This reflects in a decrease of the double occupancy  $\langle n_{i,\uparrow} \hat{n}_{i,\downarrow} \rangle$ . Furthermore the occupations become fractional and approach 1/2 for large interactions. The fractional occupation of non-interacting Bloch states indicates that bonding and antibonding states become simultaneously occupied as electron-hole pairs are formed to screen the interaction.

## 2. Local approximation and ACA

We can define impurities, that contain more than one site of the Hubbard ring Eq. (50). In the following  $N_A$  will denote the number of spin-orbitals per impurity, so that the density-matrix functional of the full interaction is approximated by a sum of  $2N/N_A$  local density-matrix

functionals

$$F^{\sum_i \hat{W}_i}[\rho] \approx \sum_{j=1}^{2N/N_A} F^{\hat{W}_{\text{imp},j}}[\rho]. \quad (55)$$

Here  $\hat{W}_{\text{imp},j}$  denotes the interaction on the  $j$ -th impurity,

$$\hat{W}_{\text{imp},j} = \sum_{i=(j-1)N_A/2+1}^{jN_A/2} \hat{W}_i. \quad (56)$$

The exact result is recovered for  $N_A = 2N$ .

The ACA is then used to evaluate the local density-matrix functionals in the sum Eq. (55).

The density-matrix functional of the system is thus approximated by

$$F^{\sum_i \hat{W}_i}[\rho] \approx \sum_{j=1}^{2N/N_A} F^{\hat{W}_{\text{imp},j}}[\rho] \quad (57)$$

$$\approx \sum_{j=1}^{2N/N_A} F_{ACA(M)}^{\hat{W}_{\text{imp},j}}[\rho]. \quad (58)$$

By varying the impurity size  $N_A$ , we can explore specifically the local approximation, the approximation in Eq. 57. The additional deviations introduced by the ACA can be controlled by increasing the truncation level  $M$ .

The rapid convergence of the ACA is demonstrated in Figure 9 for a half-filled 10-site Hubbard ring with  $U/t = 5$ . For a truncation level  $M = 3$ , the relative difference of the density-matrix functional is less than  $10^{-3}$ .

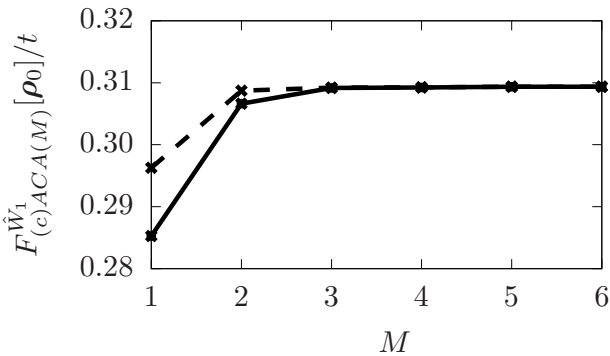


FIG. 9. Convergence of the density-matrix functional for the exact ground-state density matrix of the half-filled 10-site Hubbard ring defined by Eq. (50)-Eq. (52) with  $U/t = 5$  for different truncations parameters  $M$  of the ACA for a single-site impurity within the local approximation. The solid line shows results for the uncorrected ACA, while the dashed line shows the results for the Müller-corrected ACA.

### 3. Local Approximation and ACA for fixed impurity sizes

In this section we explore the local approximation and the ACA for a half-filled 24-site Hubbard ring. A system of this size is beyond the reach of exact diagonalization methods. We compare to the exact solutions of the Bethe ansatz equations<sup>56,57</sup>, which have been solved numerically.

The ground state is obtained by minimizing the energy

$$E_{0,N_A,ACA(M)} = \min_{\substack{\rho \\ 0 \leq \rho \leq 1, \\ \text{Tr}(\rho) = N_e}} \left\{ \text{Tr}[\rho h] + \sum_{j=1}^{2N/N_A} F_{ACA(M)}^{\hat{W}_{\text{imp},j}}[\rho] \right\}, \quad (59)$$

for the local approximation and the ACA consistent with Eq. (58).

We restricted the density matrix to be non-magnetic and translational symmetric along the ring. This restriction fixes the natural orbitals as momentum eigenstates.

As shown in Fig. 10, the ACA converges rapidly with increasing truncation level  $M$ . Already for  $M = 2$ , the deviation introduced by the ACA is smaller than the changes incurred by different impurity sizes, namely  $N_A = 2$  and  $N_A = 4$ . The latter changes are a result of the local approximation.

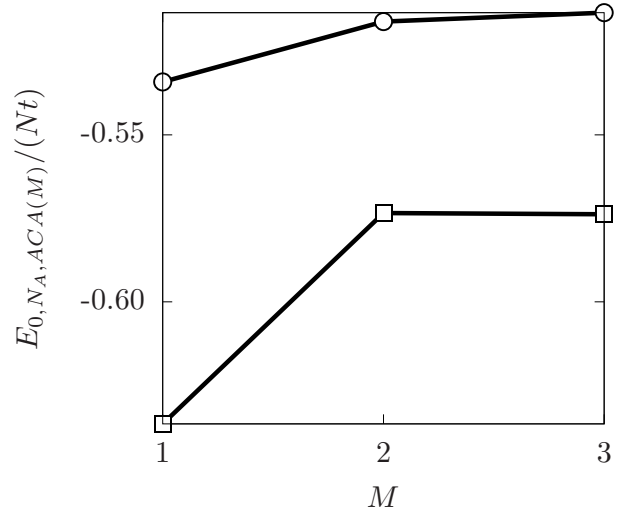


FIG. 10. Convergence of the ground-state energy  $E_{0,N_A,ACA(M)}$  of the half-filled 24-site Hubbard ring defined by Eq. (50)-Eq. (52) with  $U/t = 5$  for different truncations parameters  $M$  of the uncorrected ACA for fixed impurity sizes of the local approximation. The impurity size  $N_A$  of the local approximation is identified by symbols: single-site impurity ( $N_A = 2$ ) with circles and two-site-impurity ( $N_A = 4$ ) with squares.



#### 4. Convergence of the local approximation

The local approximation has been explored using impurities with different sizes. The results are shown in Fig. 11 for the single-site impurity and in Fig. 12 for the two-site impurity.

In Fig. 11 we can see that the overall features are reproduced already in the local approximation with the single site impurity. The interaction is screened gradually with increasing interaction strength. As a result the interaction energy shrinks again after the initial rise. The screening can be attributed to the formation of electron-hole pairs. The resulting depletion of bonding states and the population of antibonding states breaks the covalent bonds. This is seen in  $\rho^{NN}$ , which is a measure for the covalent bonding. The total energy changes its slope gradually.

The gradual transition from an uncorrelated to the large interaction limit differs from the Hartree-Fock approximation, which exhibits an abrupt transition from a state with covalent bonds to an antiferromagnetic broken symmetry states.

The comparison of the local approximation with a single-site impurity, Fig. 11, and with the two-site impurity, Fig. 12, demonstrates that the local approximation converges rapidly to the correct result, when the impurity size is increased.

### V. CONCLUSION

We introduced a method, which we call adaptive cluster approximation (ACA), to evaluate the density-matrix functional in the local approximation. The ACA leads to small truncation errors for a cluster approximation. Finite clusters, in turn, are required for the evaluation of the density-matrix functional using Levy's constrained search algorithm or other advanced approaches with an unfavourable scaling of the computational complexity. Thus, it is an important step towards the use of advanced density-matrix functionals in first-principles calculations.

Specifically, the ACA is used for describing an interacting impurity in contact with a non-interacting bath. The ACA rests on a unitary transformation of the density matrix in the bath, which limits the direct hybridization of the impurity to an inner bath with only few sites. This procedure be applied repeatedly, which brings the density matrix into a banded form, which is suitable for truncation. For the lowest possible truncation, that is one effective bath site, and a single interacting site the ACA is equivalent to the two-level approximation of Töws et al.<sup>34</sup>.

An effective correction scheme has been presented, which reduces the build-up of truncation errors during optimization of the density matrix. These deviations result from the absence of constraining forces on the corresponding density matrix elements. This correction scheme uses parameterized functionals to embed the

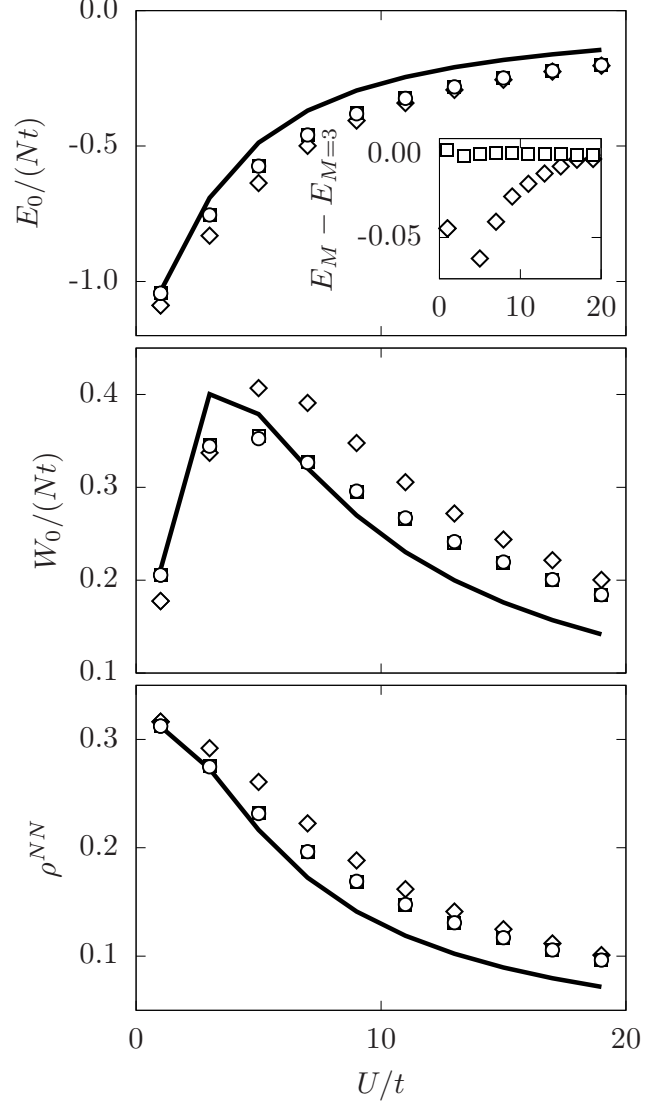


FIG. 11. Ground-state energy  $E_0$ , interaction energy  $W_0$  and nearest-neighbor density matrix elements  $\rho^{NN}$  of the ground state within the *one-site* local approximation ( $N_A = 2$ , symbols) and the exact ground state (solid line) of the half-filled 24-site Hubbard ring defined Eq. (50)-(52). The density-matrix functionals in the local approximation have been obtained using the ACA with the truncation parameters  $M = 1$  (diamonds),  $M = 2$  (squares) and  $M = 3$  (circles). The inset in the first graph shows the energy difference between lower truncations levels and  $M = 3$ .

truncated cluster into a larger effective system.

The performance of the ACA has been explored for the SIAM and – in combination with the local approximation – to the Hubbard ring. The results show that both the ACA and the local approximation converge rapidly. For the ACA the control parameter is the truncation level.

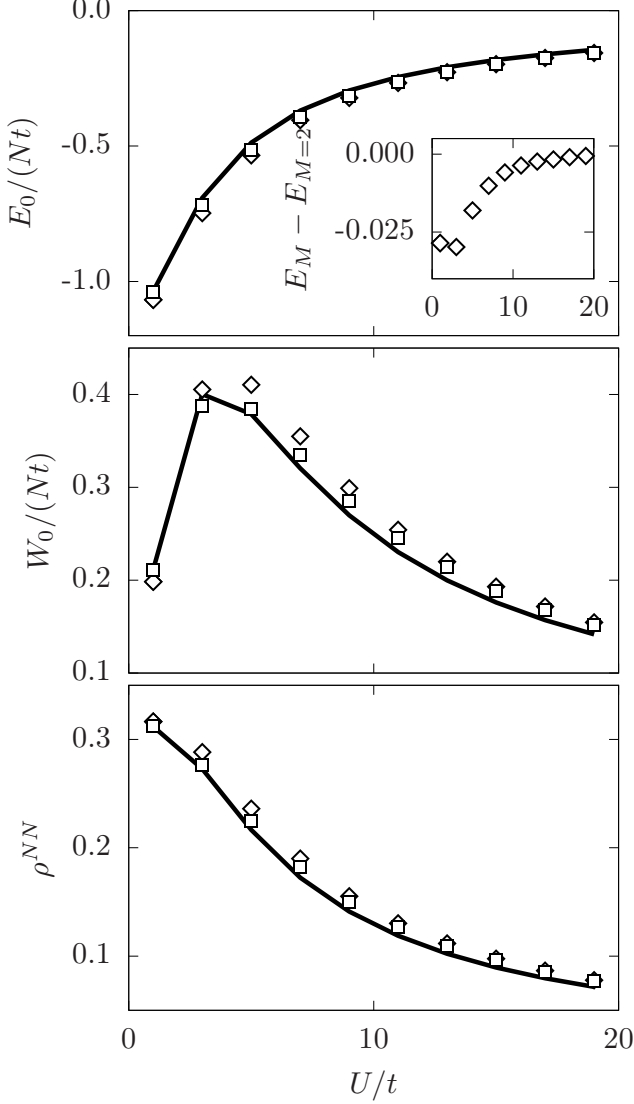


FIG. 12. Ground-state energy  $E_0$ , interaction energy  $W_0$  and nearest-neighbor density-matrix elements  $\rho^{NN}$  of the ground state within the *two-site* local approximation ( $N_A = 4$ , symbols) and the exact ground state (solid line) of the half-filled 24-site Hubbard ring defined Eq. (50)-(52). The density-matrix functionals in the local approximation have been obtained using the ACA with the given truncation parameters  $M = 1$  (diamonds) and  $M = 2$  (squares). The inset in the first graph shows the energy difference between truncation levels  $M = 1$  and  $M = 2$ .

For the local approximation it is the size of the impurity.

An important guidance for the convergence of the ACA is given by the spectrum of occupations of the bath density matrix. The truncation level for the ACA can be estimated from the number of sets of degenerate occupations. Given a finite number  $M$  of sets with degenerate

occupations, the ACA becomes exact for a finite truncation level  $M$ .

The ACA in combination with the local approximation exhibits linear computational complexity in the total system size. Thus it is one contribution towards taming the dimensional bottleneck which is haunting many-particle physics. The linear complexity paves the way for the inclusion of explicit electron correlation in density-functional-based calculations via the general formulation of DFT+rDMFT<sup>33</sup>.

## ACKNOWLEDGMENTS

Financial support from the Deutsche Forschungsgemeinschaft through FOR1346 (project 9) is gratefully acknowledged.

### Appendix A: Construction of the transformation of one-particle basis

#### 1. Construction of one unitary transformation step

We iteratively construct the unitary transformation of the bath states discussed in section II C 2 such that the one-particle reduced density matrix is a band matrix with a minimal bandwidth as given in Eq. (25). In this section we describe one iteration step. For that purpose, we write the one-particle reduced density matrix in block-form as in Eq. (20),

$$\rho = \begin{pmatrix} \rho_{AA} & \rho_{AB} \\ \rho_{AB}^\dagger & \rho_{BB} \end{pmatrix} = \begin{pmatrix} \rho_{AA} & \rho_{AB_1} & \rho_{AC_1} \\ \rho_{AB_1}^\dagger & \rho_{B_1B_1} & \rho_{B_1C_1} \\ \rho_{AC_1}^\dagger & \rho_{B_1C_1}^\dagger & \rho_{C_1C_1} \end{pmatrix}, \quad (\text{A1})$$

where the block  $A$  consists of  $N_A$  interacting states making up the impurity. The block  $B_1$  contains  $N_{B_1}$  states and the block  $C_1$  the remaining  $N_{C_1}$  states.

Transforming the one-particle basis with a block-diagonal unitary transformation defined in Eq. (21)

$$U = \begin{pmatrix} \mathbf{1}_{N_A} & \mathbf{0} \\ \mathbf{0} & U_B \end{pmatrix} = \begin{pmatrix} \mathbf{1}_{N_A} & \mathbf{0} & \mathbf{0} \\ \mathbf{0} & U_{B_1B_1} & U_{B_1C_1} \\ \mathbf{0} & U_{C_1B_1} & U_{C_1C_1} \end{pmatrix} \quad (\text{A2})$$

gives the transformed density matrix

$$\tilde{\rho} = U^\dagger \rho U = \begin{pmatrix} \rho_{AA} & \tilde{\rho}_{AB_1} & \tilde{\rho}_{AC_1} \\ \tilde{\rho}_{AB_1}^\dagger & \tilde{\rho}_{B_1B_1} & \tilde{\rho}_{B_1C_1} \\ \tilde{\rho}_{AC_1}^\dagger & \tilde{\rho}_{B_1C_1}^\dagger & \tilde{\rho}_{C_1C_1} \end{pmatrix}, \quad (\text{A3})$$

where  $\tilde{\rho}_{AC_1} = \rho_{AB_1} U_{B_1C_1} + \rho_{AC_1} U_{C_1C_1}$ .

The unitary matrix  $U_B$  is thus defined by

$$\rho_{AB_1} U_{B_1C_1} + \rho_{AC_1} U_{C_1C_1} = \mathbf{0}. \quad (\text{A4})$$

This equation has the form of a bi-orthogonality condition. The matrices  $\rho_{AB_1}$  and  $\rho_{AC_1}$  define a set of  $N_A$  vectors  $\mathbf{a}_i$  of dimension  $N_A + N_{B_1}$ . The matrices  $U_{B_1C_1}$ ,

$U_{B_1 B_1}$  and  $U_{C_1 C_1}$  are then obtained from a second set of vectors  $\mathbf{b}_i$ , which are chosen orthonormal among each other and pairwise orthogonal to the first set, i.e.

$$\mathbf{a}_i \mathbf{b}_j = 0 \quad \text{and} \quad \mathbf{b}_i \mathbf{b}_j = \delta_{i,j}. \quad (\text{A5})$$

We obtain the vectors  $\mathbf{b}_j$  from a set of linearly independent vectors of dimension  $N_{B_1} + N_{C_1}$  by first projecting out the vectors  $\mathbf{a}_i$ . In a second step, the resulting vectors are orthonormalized among each other using a Gram-Schmidt procedure.

The rank of the matrix  $(\rho_{AB_1} \rho_{AC_1})$  has to be identical to the rank of  $\tilde{\rho}_{AB_1}$ . Thereby the lower bound of the number of states  $N_{B_1}$  in block  $B_1$  is given by the rank of  $(\rho_{AB_1} \rho_{AC_1})$ , which is equal to or smaller than the number of interacting states  $N_A$ .

For an efficient minimization over the one-particle reduced density matrix in Eq. (6) or Eq. (8) derivatives of the density-matrix functional with respect to the density matrix are essential. With the Gram-Schmidt-like orthogonalisation used in the transformation of the density matrix all derivatives are accessible in a computationally efficient way.

As result we obtain a unitary transformation  $U$  of the one-particle basis, that brings any given one-particle reduced density matrix into the form

$$\tilde{\rho} = U^\dagger \rho U = \begin{pmatrix} \rho_{AA} & \tilde{\rho}_{AB_1} & 0 \\ \tilde{\rho}_{AB_1}^\dagger & \tilde{\rho}_{B_1 B_1} & \tilde{\rho}_{B_1 C_1} \\ 0 & \tilde{\rho}_{B_1 C_1}^\dagger & \tilde{\rho}_{C_1 C_1} \end{pmatrix}. \quad (\text{A6})$$

The interacting one-particle states can only have non-zero one-particle density matrix elements with each other and with the  $N_{B_1} \leq N_A$  non-interacting states of the first level effective bath.

## 2. Iterated transformations

The construction scheme for the unitary transformation of the previous section can now be applied iteratively. For that purpose we only consider the states from block  $B_1$  and  $C_1$ , i.e. the submatrix of the transformed density matrix in Eq. (A6)

$$\tilde{\rho}_{B_1 \cup C_1} = \begin{pmatrix} \tilde{\rho}_{B_1 B_1} & \tilde{\rho}_{B_1 C_1} \\ \tilde{\rho}_{B_1 C_1}^\dagger & \tilde{\rho}_{C_1 C_1} \end{pmatrix}. \quad (\text{A7})$$

The block  $C_1$  is divided into a block  $B_2$  with

$$N_{B_2} = \text{rk}(\tilde{\rho}_{B_1 C_1}) \leq N_{B_1} \leq N_A \quad (\text{A8})$$

states as the second level effective bath and a block  $C_2$  with the remaining states. We arrive at the initial situation analogously to Eq. (A1), i.e.

$$\tilde{\rho}_{B_1 \cup C_1} = \begin{pmatrix} \tilde{\rho}_{B_1 B_1} & \tilde{\rho}'_{B_1 B_2} & \tilde{\rho}'_{B_1 C_2} \\ (\tilde{\rho}_{B_1 B_2})^\dagger & \tilde{\rho}'_{B_2 B_2} & \tilde{\rho}'_{B_2 C_2} \\ (\tilde{\rho}_{B_1 C_2})^\dagger & (\tilde{\rho}'_{B_2 C_2})^\dagger & \tilde{\rho}_{C_2 C_2} \end{pmatrix}. \quad (\text{A9})$$

Now we can apply the scheme given in the previous section to construct the matrix

$$U_2 = \begin{pmatrix} \mathbf{1}_{N_{B_1}} & 0 \\ 0 & U_{B_2} \end{pmatrix} = \begin{pmatrix} \mathbf{1}_{N_{B_1}} & 0 & 0 \\ 0 & U_{B_2 B_2} & U_{B_2 C_2} \\ 0 & U_{C_2 B_2} & U_{C_2 C_2} \end{pmatrix}, \quad (\text{A10})$$

by solving the equation

$$\tilde{\rho}'_{B_1 B_2} U_{B_2 C_2} + \tilde{\rho}'_{B_1 C_2} U_{C_2 C_2} = 0. \quad (\text{A11})$$

The construction yields the unitary matrix that transforms  $\tilde{\rho}_{B_1 \cup C_1}$  to

$$U_2^\dagger \tilde{\rho}_{B_1 \cup C_1} U_2 = \begin{pmatrix} \tilde{\rho}_{B_1 B_1} & \tilde{\rho}_{B_1 B_2} & 0 \\ \tilde{\rho}_{B_1 B_2}^\dagger & \tilde{\rho}_{B_2 B_2} & \tilde{\rho}_{B_2 C_2} \\ 0 & \tilde{\rho}_{B_2 C_2}^\dagger & \tilde{\rho}_{C_2 C_2} \end{pmatrix}. \quad (\text{A12})$$

Combining the two unitary transformations  $U$  from Eq. (A6) and  $U_2$  from Eq. (A10) yields

$$\tilde{\rho} = \begin{pmatrix} \mathbf{1}_{N_A} & 0 \\ 0 & U_2^\dagger \end{pmatrix} U^\dagger \rho U \begin{pmatrix} \mathbf{1}_{N_A} & 0 \\ 0 & U_2 \end{pmatrix} \quad (\text{A13})$$

$$= \begin{pmatrix} \rho_{AA} & \tilde{\rho}_{AB_1} & 0 & 0 \\ \tilde{\rho}_{AB_1}^\dagger & \tilde{\rho}_{B_1 B_1} & \tilde{\rho}_{B_1 B_2} & 0 \\ 0 & \tilde{\rho}_{B_1 B_2}^\dagger & \tilde{\rho}_{B_2 B_2} & \tilde{\rho}_{B_2 C_2} \\ 0 & 0 & \tilde{\rho}_{B_2 C_2}^\dagger & \tilde{\rho}_{C_2 C_2} \end{pmatrix}. \quad (\text{A14})$$

Iterating this scheme leads to the band matrix given in Eq. (25), where the upper bound for the bandwidth is given by the number of interacting states  $N_A$ . The  $n$ -th order effective bath  $B_n$  consists of  $N_{B_n}$  states and the relation  $N_A \geq N_{B_1} \geq N_{B_2} \geq \dots$  holds.

## Appendix B: Exact decoupling

Here we prove a relation between the eigenvalue spectrum of the bath-density matrix and the discarded weight discussed in sec. II C 5: If the eigenvalue spectrum of the bath-density matrix consists of  $N$  distinct values with a  $n_j$ -fold degeneracy each, then there is a number of effective bath states  $N_B \leq \sum_{j=1}^N \min(n_j, N_A)$  for which the discarded weight  $\sigma_{N_A + N_B}(\tilde{\rho})$  of the transformed density matrix  $\tilde{\rho}$  vanishes.

To prove this relation, we write the one-particle reduced density matrix  $\rho$  in a block-form as in Eq. (20)

$$\rho = \begin{pmatrix} \rho_{AA} & \rho_{AB} \\ \rho_{AB}^\dagger & \rho_{BB} \end{pmatrix}, \quad (\text{B1})$$

where  $\rho_{AA} \in \mathbb{C}^{N_A \times N_A}$  and  $\rho_{BB} \in \mathbb{C}^{N_x - N_A \times N_x - N_A}$ . By diagonalization of the bath-density matrix  $\rho_{BB}$  any density matrix can be transformed to the shape

$$\tilde{\rho} = U^\dagger \rho U = \begin{pmatrix} \rho_{AA} & \tilde{\rho}_{\lambda, AB} \\ \tilde{\rho}_{\lambda, AB}^\dagger & \text{diag}(\lambda_1, \dots, \lambda_{N_x - N_A}) \end{pmatrix}. \quad (\text{B2})$$

Here  $\text{diag}(\lambda_1, \dots, \lambda_{N_x - N_A})$  stands for the real matrix with the ordered eigenvalues  $\lambda_1, \dots, \lambda_{N_x - N_A}$  of  $\rho_{BB}$  on the diagonal. No additional properties of  $\tilde{\rho}_{\lambda, AB}$  are assumed.

Thus the following discussion is valid for any hermitian matrix  $\rho$ .

Now we assume that the eigenvalue spectrum of the bath density matrix  $\rho_{BB}$  consists of  $N$  distinct values  $\Lambda_1, \dots, \Lambda_N$  with the degeneracies  $n_1, \dots, n_N$ , i.e.  $\Lambda_1 = \lambda_1 = \dots = \lambda_{n_1}$ . If we consider a single set of degenerate eigenvalues with the index  $j \in \{1, \dots, N\}$  we can write the rows and columns corresponding to this set as

$$\tilde{\rho} = \left( \begin{array}{c|c|c} \rho_{AA} & \dots & \tilde{\rho}_{\lambda, AB_j} & \dots \\ \vdots & \dots & \mathbf{0} & \dots \\ \hline \tilde{\rho}_{\lambda, AB_j}^\dagger & \mathbf{0} & \Lambda_j \mathbf{1}_{n_j \times n_j} & \mathbf{0} \\ \vdots & \dots & \mathbf{0} & \dots \end{array} \right), \quad (\text{B3})$$

with  $\tilde{\rho}_{\lambda, AB}$  in Eq. (B2) written as  $\tilde{\rho}_{\lambda, AB} = (\tilde{\rho}_{\lambda, AB_1} \dots \tilde{\rho}_{\lambda, AB_N})$ .

Within each  $n_j$ -dimensional eigenspace for the eigenvalue  $\Lambda_j$  we can perform a unitary transformation  $U'_j$ , i.e. in total the block-diagonal unitary transformation  $U'$

$$U' = \left( \begin{array}{c|c|c|c} \mathbf{1}_{N_A} & \mathbf{0} & \dots & \\ \mathbf{0} & U'_1 & \mathbf{0} & \dots \\ \vdots & & \ddots & \\ \mathbf{0} & \dots & \mathbf{0} & U'_N \end{array} \right). \quad (\text{B4})$$

$$\tilde{\rho}' = (U')^\dagger \tilde{\rho} U' = \left( \begin{array}{c|c|c} \rho_{AA} & \dots & \tilde{\rho}'_{\lambda, AB_j} & \mathbf{0} & \dots \\ \vdots & \dots & \mathbf{0} & \mathbf{0} & \dots \\ \hline (\tilde{\rho}'_{\lambda, AB_j})^\dagger & \mathbf{0} & \Lambda_j \mathbf{1}_{n'_j \times n'_j} & \mathbf{0} & \mathbf{0} \\ \mathbf{0} & \mathbf{0} & \mathbf{0} & \Lambda_j \mathbf{1}_{n_j - n'_j \times n_j - n'_j} & \mathbf{0} \\ \vdots & \dots & \mathbf{0} & \mathbf{0} & \dots \end{array} \right). \quad (\text{B6})$$

Basis states corresponding to blocks with  $\Lambda_j \mathbf{1}_{n_j - n'_j \times n_j - n'_j}$  do not couple to other basis states and can be neglected.

So that the upper bound for number of the remaining bath basis states is given by

$$\sum_{j=1}^N n'_j = \sum_{j=1}^N \min \left[ n_j, rk(\tilde{\rho}_{\lambda, AB_j}) \right]. \quad (\text{B7})$$

We have shown that an arbitrary density matrix with an impurity of  $N_A$  states and  $N$  disjoint sets of  $n_j$ -fold degenerate eigenvalues of the bath-density matrix can be exactly decoupled if the number of effective bath basis states is at least  $\sum_{j=1}^N \min \left[ n_j, rk(\tilde{\rho}_{\lambda, AB_j}) \right]$ . The upper bound is given by  $\sum_{j=1}^N \min(n_j, N_A)$ , when all  $\tilde{\rho}_{\lambda, AB_j}$  have full column rank.

In the case of  $N_A = 2$ , that is a two-spin-orbital impurity, and a non-spin-polarized density matrix, i.e.  $n_j \geq 2$ , we obtain an upper bound for the number of effective bath sites equal to the number  $N$  of disjoint sets of de-

The unitary matrices  $U'_j$  of the separate blocks are now chosen, so that they transform  $\tilde{\rho}_{\lambda, AB_j}$  in Eq. (B3) as

$$\begin{pmatrix} \tilde{\rho}'_{\lambda, AB_j} & \mathbf{0} \end{pmatrix} = \tilde{\rho}_{\lambda, AB_j} U'_j, \quad (\text{B5})$$

where  $\tilde{\rho}'_{\lambda, AB_j}$  should have the least possible number of columns, that we denote with  $n'_j$ .

The upper bound for the number of columns of the matrix  $\tilde{\rho}'_{\lambda, AB_j}$  can be deduced as follows:

- If  $n_j \leq N_A$ , then  $n'_j = rk(\tilde{\rho}_{\lambda, AB_j}) \leq n_j$  holds.
- In case  $n_j > N_A$ , we have  $n'_j = rk(\tilde{\rho}_{\lambda, AB_j}) \leq N_A$ .

We then obtain the form

generate eigenvalues of the bath density matrix.

Because of the construction of the unitary transformations via a Gram-Schmidt-like orthogonalisation scheme, the ACA does not rely on a degeneracy of the eigenvalues of the bath-density matrix, which would be problematic in a numerical treatment.

If the eigenvalues of the bath-density matrix are not degenerate within groups, but form  $N$  clusters with small but finite spreads, the ACA transformation results in a finite, but very small discarded weight after  $N$  effective bath levels. As discussed in sec. II C 3 a small discarded weight results in a small truncation error.

### Appendix C: Single-impurity Anderson model in additional parameter regimes

In appendix C 1 we investigate the dependence of the SIAM defined in section IV A 1 on the on-site energy of the impurity  $\epsilon_f$ . In the subsequent section C 2 we explore the dependence on the bath bandwidth.

### 1. Impurity on-site-energy dependence

*a. Exact results* The dependence of the exact ground state and the ground state in the Hartree-Fock approximation on the impurity on-site energy  $\epsilon_f$  for the single-impurity Anderson model defined by Eq. (42)-(47) and  $N_{\text{bath}} = 11$ ,  $U/t = 8$ ,  $t > 0$ ,  $V/t = 0.4$  is shown in Fig. 13.

The behaviour of this model for different impurity on-site energies  $\epsilon_f$  can be separated in three regions, depending on the relation of the on-site energy to the Fermi energy of the bath  $\epsilon_{F,\text{bath}} \approx 0.28t$ .

- For  $\epsilon_f + U \ll \epsilon_{F,\text{bath}}$ , the impurity is doubly occupied  $n_f \approx 2$ . The interaction energy takes the maximal possible value  $W_{\text{max}} = U$ .
- The range  $\epsilon_f < \epsilon_{F,\text{bath}}$  and  $\epsilon_{F,\text{bath}} < \epsilon_f + U$  is the Kondo regime. The impurity is approximately half filled, i.e.  $n_f \approx 1$ . The charge fluctuation on the impurity  $\langle n_f^2 \rangle - \langle n_f \rangle^2$ , is small in this region, so that the ground-state wave function has only a negligible contribution from states that are empty or doubly occupied on the impurity. In this region, the impurity can be described by an effective local spin-1/2-moment, that is coupled to the bath. This situation is identical to the Kondo model<sup>61</sup>.
- For  $\epsilon_f > \epsilon_{F,\text{bath}}$ , the impurity is nearly empty.

The three energy regions are separated by mixed-valence regions. Here the impurity occupation switches rapidly from one integral occupation to another and the charge fluctuations on the impurity are thus large.

The unrestricted Hartree-Fock approximation is exact in the limits of a doubly occupied impurity  $\epsilon_f \rightarrow -\infty$  and an empty impurity  $\epsilon_f \rightarrow \infty$ . In the intermediate region shown in Fig. 13 it qualitatively reproduces the three distinct regions, but suffers from an unphysical spin-symmetry breaking with a finite magnetic moment on the impurity  $m_f > 0$  in the Kondo-regime.

Fig. 14 shows the eigenvalue spectrum of the bath density matrix of the exact ground state as function of the impurity on-site energy. Similarly to the interaction-strength dependence discussed in section IV A 2 we find here at most three distinct clusters of eigenvalues with very small spread, so that we expect the ACA with three effective bath sites, i.e.  $M = 3$ , to converge to the exact ground state within the convergence tolerance of the numerical minimization.

*b. Full minimization over the one-particle reduced density matrix* Let us compare the ACA with the exact result and the Hartree-Fock approximation. The ACA with truncation level  $M = 3$  is again exact within the numerical precision of the solver for the density-matrix functional, and will not be discussed further in this section. Rather, we concentrate on the performance of the low truncation levels  $M = 1$  and  $M = 2$ .

The deviations of the ACA from the exact results are shown in Fig. 15.

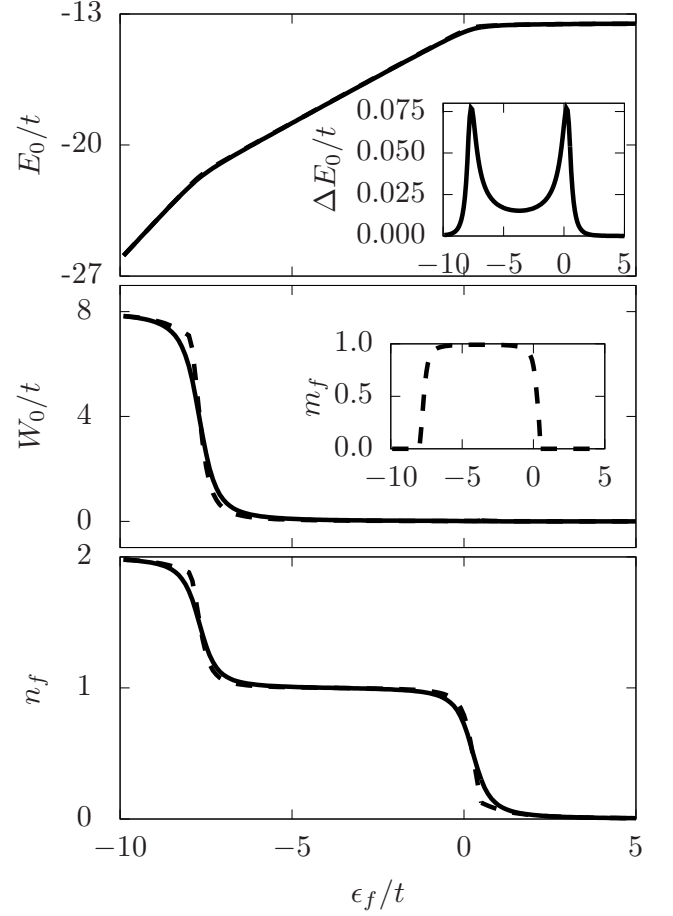


FIG. 13. Ground-state energy  $E_0$ , interaction energy  $W_0$  and impurity occupation  $n_f$  of the exact ground state (solid lines) and the unrestricted Hartree-Fock ground state (dashed lines) of the Hamiltonian defined Eq. (42)-(47) with  $N_{\text{bath}} = 11$ ,  $U/t = 8$ ,  $t > 0$ ,  $V/t = 0.4$  at half filling. The inset in the first graph shows the difference  $\Delta E_0 = E_{0,\text{HF}} - E_0$  between the ground-state energy in the Hartree-Fock approximation and the exact result. The inset in the second graph shows the magnetic moment  $m_f = n_{f,\uparrow} - n_{f,\downarrow}$  of the impurity within the Hartree-Fock approximation.

The ACA with low truncation levels  $M = 1$  and  $M = 2$  and the Hartree-Fock approximation describe the system well in the energy regions with the empty and the doubly occupied impurity. In the Kondo regime, the Hartree-Fock approximation describes the interaction energy well, but the predicted state is a broken symmetry state with a magnetized impurity. The ACA describes the physical state of Kondo regime correctly.

The good description of the Kondo regime indicates that the ACA copes well with static correlation, that is with states that cannot be represented well with a single Slater determinant. The ACA inherits this feature from the constrained search, which constructs the density-matrix functional from a multi-configuration wave function.

The largest deviations occur in the mixed-valence



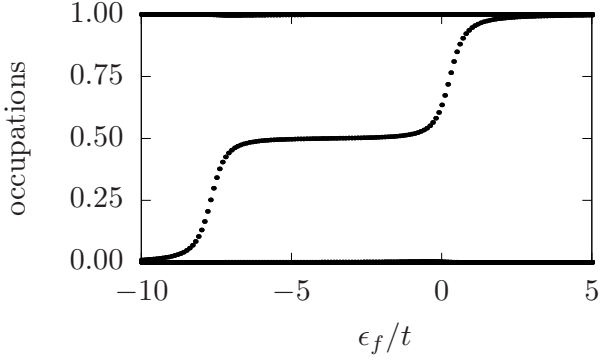


FIG. 14. Eigenvalue spectrum (occupations) of the bath density matrix  $\rho_{BB}$  of the exact ground state of the Hamiltonian defined Eq. (42)-(47) with  $N_{\text{bath}} = 11$ ,  $U/t = 8$ ,  $t > 0$ ,  $V/t = 0.4$  at half filling.

regimes at  $\epsilon_f = \epsilon_{F,\text{bath}} - U \approx -7.7t$  and  $\epsilon_f = \epsilon_{F,\text{bath}} \approx 0.28t$ . Even for low truncation levels such as  $M = 1$  and  $M = 2$ , the impurity occupation and the total energy deviate only by about 3 % from the exact value. The deviations in the total energy are one order of magnitude smaller than those of the interaction energy.

The Müller correction (section IID) of the ACA improves the uncorrected ACA considerably, in particular in the mixed-valence regime where the deviations are largest.

## 2. Bandwidth dependence

*c. Exact results* As discussed in section IIC5 the ACA is exact for a SIAM in the limit of a vanishing bath bandwidth  $t \rightarrow 0$  and in the limit of widely separated discrete bath levels  $t \rightarrow \infty$ . By varying the hopping  $t$  in the bath, which is proportional to the bath bandwidth, we investigate these two limits. The dependence of the exact ground state and the ground state in the Hartree-Fock approximation on the bath hopping parameter  $t$  for the single-impurity Anderson model defined by Eq. (42)-(47) and  $N_{\text{bath}} = 11$ ,  $U/V = 5$ ,  $V > 0$ ,  $\epsilon_f/V = -1$  is shown in Fig. 16. The exact total energy is approximately linear with the bath hopping parameter, because it is dominated by the one-particle energy of the bath. In the limit of degenerate bath levels,  $t \rightarrow 0$ , the Fermi energy of the bath vanishes  $\epsilon_{F,\text{bath}} = 0$ . In this limit the system is close to the transition from the singly occupied to the empty impurity, because of  $\epsilon_f + U \gg \epsilon_{F,\text{bath}}$  and  $\epsilon_f < \epsilon_{F,\text{bath}}$ .

Increasing the bath hopping  $t$  increases the distance of the bath-Fermi energy  $\epsilon_{F,\text{bath}} \approx 0.28t$  to the impurity on-site energy  $\epsilon_f = -V$ , so that impurity occupation increases (see also Fig. 16).

In the limit of widely separated discrete bath levels,  $t \rightarrow \infty$ , the impurity is doubly occupied and the interaction energy maximal,  $W_0 = U$ .

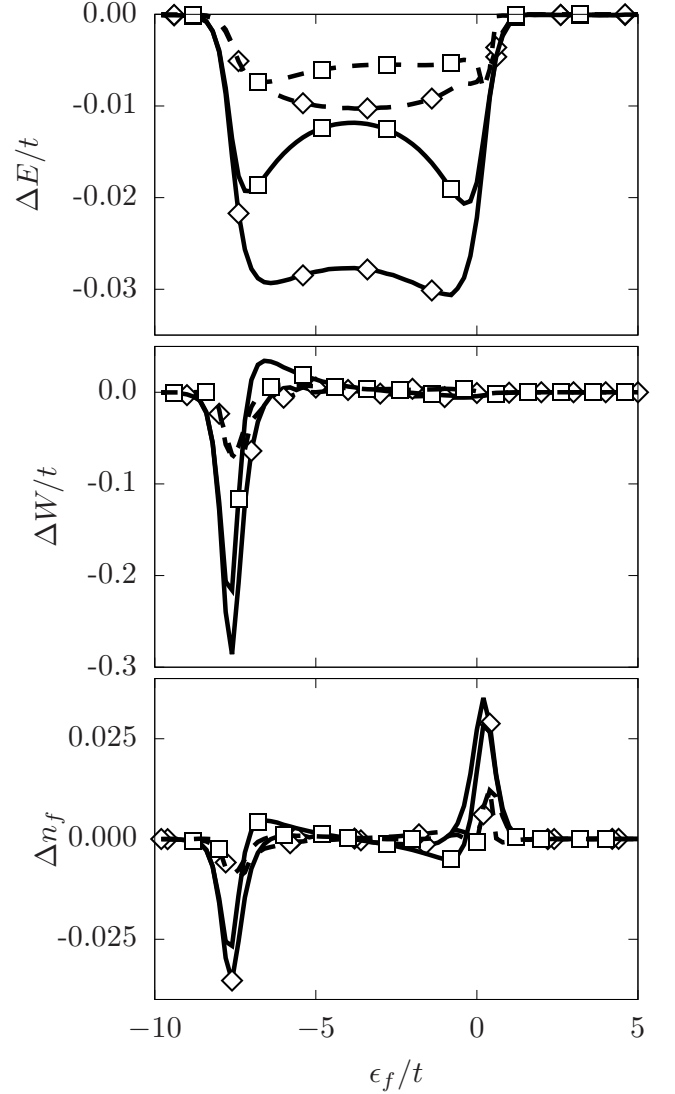


FIG. 15. Deviation of the ground-state energy  $\Delta E = E_{(c)ACA(M)} - E_0$ , interaction energy  $\Delta W = W_{(c)ACA(M)} - W_0$  and impurity occupation  $\Delta n_f = n_{f,(c)ACA(M)} - n_f$  between the ground state within the (corrected) adaptive cluster approximation and the exact ground state. The corresponding exact results are shown in Fig. 13. The Hamiltonian is defined in Eq. (42)-(47) with the parameters  $N_{\text{bath}} = 11$ ,  $U/t = 8$ ,  $t > 0$ ,  $V/t = 0.4$  and at half filling. Solid lines correspond to the uncorrected ACA and dashed lines to the Müller-corrected ACA results. Truncation with  $M = 1$  (solid line with diamonds) and  $M = 2$  (solid line with squares). The results for  $M = 3$  are not shown, because they agree with the exact results within the convergence criteria.

Also in this parameter range the unrestricted Hartree-Fock approximation suffers from an unphysical spin-symmetry breaking. It becomes exact in the limit of widely separated discrete bath levels.

The spectrum of the bath density matrix of the exact ground state in Fig. (17), also shows three distinct

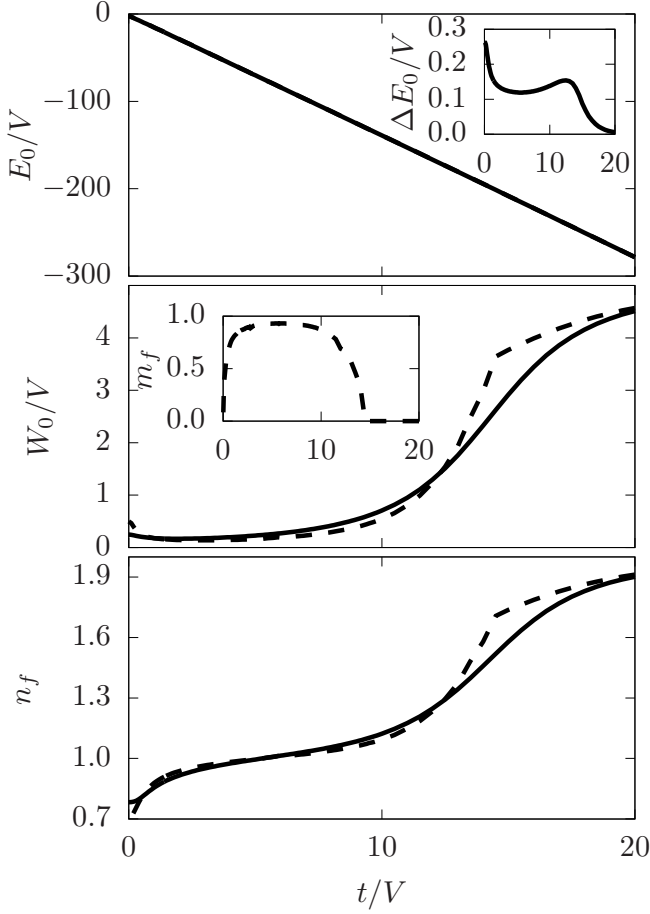


FIG. 16. Ground-state energy  $E_0$ , interaction energy  $W_0$  and impurity occupation  $n_f$  of the exact ground state (solid lines) and the unrestricted Hartree-Fock ground state (dashed lines) of the Hamiltonian defined Eq. (42)-(47) with  $N_{\text{bath}} = 11$ ,  $U/V = 5$ ,  $V > 0$ ,  $\epsilon_f/V = -1$  at half filling. The inset in the first graph shows the difference  $\Delta E_0 = E_{0,\text{HF}} - E_0$  between the ground-state energy in the Hartree-Fock approximation and the exact result. The inset in the second graph shows the magnetic moment  $m_f = n_{f,\uparrow} - n_{f,\downarrow}$  of the impurity within the Hartree-Fock approximation.

clusters of eigenvalues for finite bath hopping parameters. Consequently the ACA with  $M = 3$  will reproduce the exact ground state within the convergence tolerance of the numerical minimization. In the limit of vanishing bath bandwidth  $t \rightarrow 0$  the cluster with fractional occupations has a large finite spread, so that the argu-

ment based on clusters of degenerate eigenvalues will not hold anymore. However the limit of vanishing bath bandwidth is already exactly described by the ACA with just one effective bath site, i.e.  $M = 1$ . This is due to the equivalence with the two-level approximation, which has been shown to be exact in this case<sup>34</sup>.

*d. Full minimization over the one-particle reduced density matrix* Figure 18 shows the deviations of the ground-state energy, interaction energy and impurity occupation within the (corrected) ACA with one and two

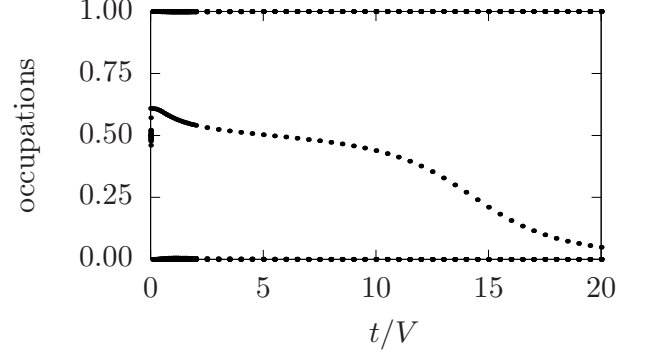


FIG. 17. Eigenvalue spectrum (occupations) of the bath density matrix  $\rho_{BB}$  of the exact ground state of the Hamiltonian defined Eq. (42)-(47) with  $N_{\text{bath}} = 11$ ,  $U/V = 5$ ,  $V > 0$ ,  $\epsilon_f/V = -1$  at half filling.

effective bath sites from the exact results. The numerical results confirm that the uncorrected ACA with one effective bath site ( $M = 1$ ) becomes exact in the limit of a vanishing bath bandwidth  $t \rightarrow 0$  and in the limit of widely separated bath levels  $t \rightarrow \infty$  as discussed in section II C 5. Even though the interaction energy varies between very small values and  $W \approx U$  in this parameter regime, we get small deviations of the interaction energy within the ACA over the whole range. Unfortunately the deviations are largest in the regime, where the impurity is approximately single occupied and the absolute value of the interaction energy is small. Also in this parameter regime we find a strong correlation between large deviations of the impurity occupation and large deviations in the total ground-state energy and interaction energy. The correction with the Müller functional reduces the deviation of the total energy by approximately a factor of two compared to the corresponding uncorrected ACA results.

\* robert.schade@tu-clausthal.de

<sup>1</sup> T. L. Gilbert, *Phys. Rev. B* **12**, 2111 (1975).

<sup>2</sup> M. Levy, *Proc. Nat'l Acad. Sci. USA* **76**, 6062 (1979).

<sup>3</sup> E. H. Lieb, *Int. J. Quantum Chem.* **24**, 243 (1983).

<sup>4</sup> P. Hohenberg and W. Kohn, *Phys. Rev.* **136**, B864 (1964).

<sup>5</sup> W. Kohn and L. J. Sham, *Phys. Rev.* **140**, A1133 (1965).

<sup>6</sup> R. López-Sandoval and G. M. Pastor, *Phys. Rev. B* **61**, 1764 (2000).

<sup>7</sup> R. G. Hennig and A. E. Carlsson, *Phys. Rev. B* **63**, 115116 (2001).

<sup>8</sup> R. López-Sandoval and G. M. Pastor, *Phys. Rev. B* **66**, 155118 (2002).

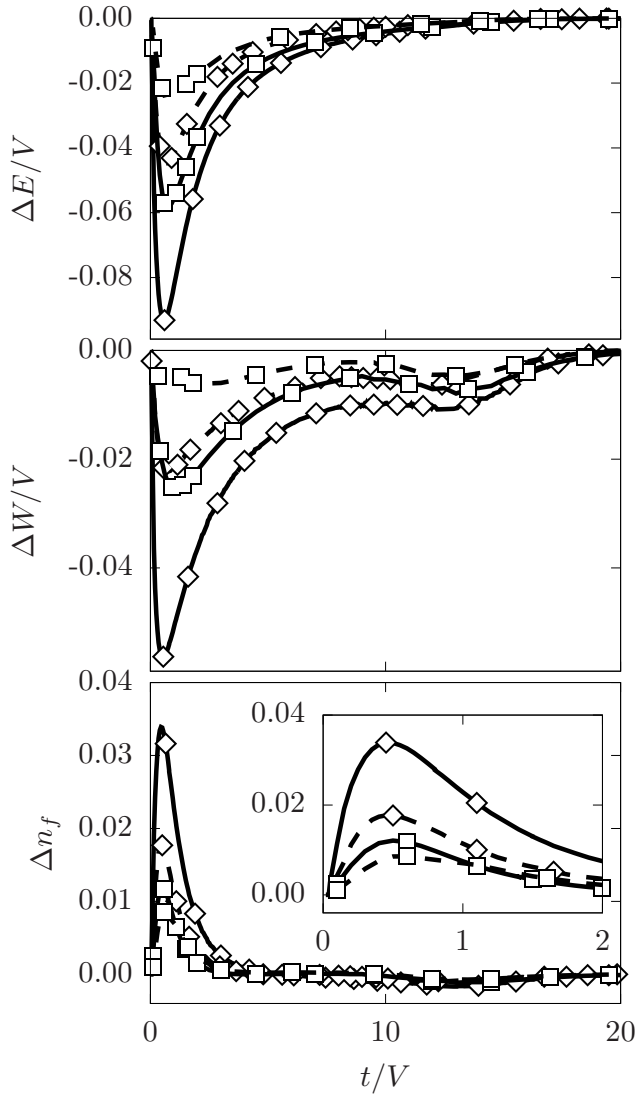


FIG. 18. Deviation of the ground-state energy  $\Delta E = E_{(c)ACA(M)} - E_0$ , interaction energy  $\Delta W = W_{(c)ACA(M)} - W_0$  and impurity occupation  $\Delta n_f = n_{f,(c)ACA(M)} - n_f$  between the ground state within the (corrected) adaptive cluster approximation and the exact ground state. The corresponding exact results are shown in Fig. 16. The Hamiltonian is defined in Eq. (42)-(47) with the parameters  $N_{\text{bath}} = 11$ ,  $U/V = 5$ ,  $V > 0$  and  $\epsilon_f/V = -1$  and at half filling. Solid lines correspond to the uncorrected ACA and dashed lines to the Müller-corrected ACA results. Truncation with  $M = 1$  (solid line with diamonds) and  $M = 2$  (solid line with squares). The results for  $M = 3$  are not shown, because they agree with the exact results within the convergence criteria.

- <sup>9</sup> R. López-Sandoval and G. M. Pastor, *Phys. Rev. B* **67**, 035115 (2003).  
<sup>10</sup> R. López-Sandoval and G. M. Pastor, *Phys. Rev. B* **69**, 085101 (2004).  
<sup>11</sup> N. N. Lathiotakis, S. Sharma, J. K. Dewhurst, F. G. Eich, M. A. L. Marques, and E. K. U. Gross, *Phys. Rev. A* **79**, 040501 (2009).

- <sup>12</sup> W. Töws and G. M. Pastor, *Phys. Rev. B* **83**, 235101 (2011).  
<sup>13</sup> C. Benavides-Riveros and J. Várrily, *Eur. Phys. J. D* **66**, 274 (2012).  
<sup>14</sup> W. Töws and G. M. Pastor, *Phys. Rev. B* **86**, 245123 (2012).  
<sup>15</sup> M. Saubanière, M. B. Lepetit, and G. M. Pastor, *Phys. Rev. B* **94**, 045102 (2016).  
<sup>16</sup> S. di Sabatino, J. A. Berger, L. Reining, and P. Romaniello, *J. Chem. Phys.* **143**, 024108 (2015).  
<sup>17</sup> E. Kamil, R. Schade, T. Pruschke, and P. E. Blöchl, *Phys. Rev. B* **93**, 085141 (2016).  
<sup>18</sup> S. Goedecker and C. J. Umrigar, *Phys. Rev. Lett.* **81**, 866 (1998).  
<sup>19</sup> V. Staroverov and G. Scuseria, *J. Chem. Phys.* **117**, 2489 (2002).  
<sup>20</sup> N. Lathiotakis and M. Marques, *J. Chem. Phys.* **128**, 184103 (2008).  
<sup>21</sup> N. N. Lathiotakis, N. Helbig, and E. K. U. Gross, *Phys. Rev. B* **75**, 195120 (2007).  
<sup>22</sup> O. Gritsenko, K. Pernal, and E. J. Baerends, *J. Chem. Phys.* **122**, 204102 (2005).  
<sup>23</sup> M. A. L. Marques and N. N. Lathiotakis, *Phys. Rev. A* **77**, 032509 (2008).  
<sup>24</sup> S. Sharma, J. K. Dewhurst, S. Shallcross, and E. K. U. Gross, *Phys. Rev. Lett.* **110**, 116403 (2013).  
<sup>25</sup> Y. Shinohara, S. Sharma, S. Shallcross, N. N. Lathiotakis, and E. K. U. Gross, *Journal of Chemical Theory and Computation* **11**, 4895 (2015), pMID: 26574277, <http://dx.doi.org/10.1021/acs.jctc.5b00661>.  
<sup>26</sup> Y. Shinohara, S. Sharma, J. K. Dewhurst, S. Shallcross, N. N. Lathiotakis, and E. K. U. Gross, *New Journal of Physics* **17**, 093038 (2015).  
<sup>27</sup> S. Di Sabatino, J. A. Berger, L. Reining, and P. Romaniello, *Phys. Rev. B* **94**, 155141 (2016).  
<sup>28</sup> M. Piris and P. Otto, *International Journal of Quantum Chemistry* **94**, 1093 (2000).  
<sup>29</sup> M. Piris, *International Journal of Quantum Chemistry* **106**, 1093 (2006).  
<sup>30</sup> M. Piris and J. M. Ugalde, *International Journal of Quantum Chemistry* **114**, 1169 (2014).  
<sup>31</sup> X. Lopez, F. Ruiperez, M. Piris, J. M. Matxain, E. Matito, and J. M. Ugalde, *Journal of Chemical Theory and Computation* **8**, 2646 (2012), pMID: 26592109, <http://dx.doi.org/10.1021/ct300414t>.  
<sup>32</sup> K. Pernal and K. J. H. Giesbertz, “Reduced density matrix functional theory (rdmft) and linear response time-dependent rdmft (td-rdmft),” in *Density-Functional Methods for Excited States*, edited by N. Ferré, M. Filatov, and M. Huix-Rotllant (Springer International Publishing, Cham, 2016) pp. 125–183.  
<sup>33</sup> P. E. Blöchl, C. F. J. Walther, and T. Pruschke, *Phys. Rev. B* **84**, 205101 (2011).  
<sup>34</sup> W. Töws and G. M. Pastor, *Phys. Rev. B* **83**, 235101 (2011).  
<sup>35</sup> A. Coleman, *Rev. Mod. Phys.* **35**, 668 (1963).  
<sup>36</sup> P.-O. Löwdin, *Phys. Rev.* **97**, 1474 (1955).  
<sup>37</sup> S. M. Valone, *The Journal of Chemical Physics* **73**, 1344 (1980).  
<sup>38</sup> T. Baldisiefen, A. Cangi, and E. K. U. Gross, *Phys. Rev. A* **92**, 052514 (2015).  
<sup>39</sup> R. Pariser and R. G. Parr, *The Journal of Chemical Physics* **21**, 466 (1953).  
<sup>40</sup> R. Pariser and R. G. Parr, *The Journal of Chemical Physics* **21**, 767 (1953).  
<sup>41</sup> J. A. Pople, *Trans. Faraday Soc.* **49**, 1375 (1953).  
<sup>42</sup> M. C. Gutzwiller, *Phys. Rev. Lett.* **10**, 159 (1963).

- <sup>43</sup> J. Hubbard, *Proc. R. Soc. Lond. A* **276**, 238 (1963).
- <sup>44</sup> J. Kanamori, *Prog. Theor. Phys.* **30**, 275 (1963).
- <sup>45</sup> F. Gebhard, *The Mott Metal-Insulator Transition: Models and Methods*, Springer Tracts in Modern Physics (Springer Berlin Heidelberg, 1997).
- <sup>46</sup> A. M. K. Müller, *Phys. Lett.* **105**, 446 (1984).
- <sup>47</sup> M. Buijse and E. Baerends, *Mol. Phys.* **100**, 401 (2002).
- <sup>48</sup> S. Sharma, J. K. Dewhurst, N. N. Lathiotakis, and E. K. U. Gross, *Phys. Rev. B* **78**, 201103 (2008).
- <sup>49</sup> C. A. Büsser, G. B. Martins, and A. E. Feiguin, *Phys. Rev. B* **88**, 245113 (2013).
- <sup>50</sup> T. Shirakawa and S. Yunoki, *Phys. Rev. B* **90**, 195109 (2014).
- <sup>51</sup> C. Lin and A. A. Demkov, *Phys. Rev. B* **88**, 035123 (2013).
- <sup>52</sup> Y. Lu, M. Höppner, O. Gunnarsson, and M. W. Haverkort, *Phys. Rev. B* **90**, 085102 (2014).
- <sup>53</sup> M. Schüler, C. Renk, and T. O. Wehling, *Phys. Rev. B* **91**, 235142 (2015).
- <sup>54</sup> P. Anderson, *Phys. Rev.* **124**, 41 (1961).
- <sup>55</sup> M. Bollhofer and Y. Notay, *Computer Physics Communications* **177**, 951 (2007).
- <sup>56</sup> H. Bethe, *Zeitschrift für Physik* **71**, 205.
- <sup>57</sup> E. H. Lieb and F. Y. Wu, *Phys. Rev. Lett.* **20**, 1445 (1968).
- <sup>58</sup> R. Car and M. Parrinello, *Phys. Rev. Lett* **55**, 2471 (1985).
- <sup>59</sup> L. Verlet, *Phys. Rev.* **159**, 98 (1967).
- <sup>60</sup> J.-P. Ryckaert, G. Ciccotti, and H. J. C. Berendsen, *J. Comput. Phys.* **23**, 327 (1977).
- <sup>61</sup> J. Kondo, *Progress of Theoretical Physics* **32**, 37 (1964).